UNIVERSITY OF OKLAHOMA

GRADUATE COLLEGE

A THESIS

SUBMITTED TO THE GRADUATE FACULTY

in partial fulfillment of the requirements for the

Degree of

MASTER OF SCIENCE

By

Kyle Twitchell

Norman, Oklahoma

2020

EXPLORING HEMOLYSIS DUE TO PARAVALVULAR LEAKAGE IN ARTIFICIAL HEART VALVES

A THESIS APPROVED FOR THE

SCHOOL OF CHEMICAL, BIOLOGICAL AND MATERIALS ENGINEERING

BY THE COMMITTEE CONSISTING OF

Dr. Edgar O'Rear, Chair

Dr. Dimitrios Papavassiliou

Dr. Vassilios Sikavitsas

Acknowledgements

I would like to start by thanking Drs. Edgar O'Rear and Dimitrios Papavassiliou, who have not only agreed to be on my defense committee, but who have also been with me from the first step of this journey until the very end. Through endless meetings and an untold number of drafts of this manuscript, they have been supportive and helpful. There is no way that this would ever have been completed without their encouragement, and now that it's finished, I'm indescribably thankful.

Dr. Vassilios Sikavitsas has agreed to be part of my committee, and for that I am also grateful, especially in light of the rather frantic and last-minute nature of the request.

Dr. Toru Maruyama provided much of the medical insight into the problems discussed herein. Without his insight, this project would have stalled.

Dr. Jichao Zhou was kind enough to send cross-sectional images of the atrial wall, which proved instrumental in the eventual construction of the model and solved a problem that I had been struggling with for years.

I would like to thank the University of Oklahoma for allowing me to use its various resources and facilities through the course of this research. It would have been impossible if not for the ability to use several key software licenses remotely.

It's 2020, and I am thankful to all the first responders, medical professionals, and front-line workers that kept the world spinning as it tried to stop.

Finally, I need to thank my family for all the love in the world. There were times when I wanted to give up, but you kept me going. Nothing means more to me than you.

Table of Contents

List of Figures:

List of Tables:

Abstract:

Artificial heart valves require a surgical suture to keep them in place. These sutures can become infected or degrade over time, which can give rise to the phenomenon of paravalvular leakage. The defect compromising flow occurs due to a gap or channel between the rim of the valve and the heart wall. Regurgitation through the separation subjects blood cells to flow conditions and stresses outside of their normal operating conditions and can cause hemolysis.

This study on paravalvular leakage of a bileaflet mitral valve prosthesis builds on previous computational work done to develop a model for hemolysis pertinent to turbulent flow. A three-dimensional model of the left atrium was used to calculate the amount of hemolysis caused by paravalvular leakage. This three-dimensional model was examined using computational fluid dynamics, in which the Kolmogorov Length Scale of the eddies involved was calculated, and the technique of eddy analysis was used to determine how much hemolysis occurs. The vast majority of the damage is found to be caused by the channel which allows paravalvular leakage, and not the flow within the atrium itself, though the amount of hemolysis predicted is lower than expected from its medical relevancy, leading to the assumption that the geometry in question needs to be altered for future work.

1. Background

Section 1.1: Medical Background

Hemolytic anemia occurs when human red blood cells (RBCs), are destroyed faster than they can be produced [1]. Even in healthy people, RBCs live on average for only 120 days, so the body must have a natural way of disposing of them. This process ends in the spleen, which filters out senescent or injured RBCs, but when it happens elsewhere in the body, the destruction of RBCs is known as hemolysis. When hemolysis outpaces new RBC growth in bone marrow, patients may experience: paleness, jaundice, dark urine, fever, weakness, dizziness, confusion, reduced stamina, enlarged liver or spleen, tachycardia, or a heart murmur [1]. Left completely untreated, hemolytic anemia can lead to life threatening heart conditions.

This anemia can be the result of genetic conditions, infections, or autoimmune diseases, but of greatest interest here is microangiopathic anemia, which is caused by flow conditions within the body. Typical values for the amount of hemoglobin in blood are around 15 g/dL [2]. There have been cases reported where microangiopathic anemia has resulted in patients with hemoglobin levels of 4.4 g/dl in extreme cases [3]. Among the most common causes of microangiopathic anemia are intravascular devices, which chiefly refers to artificial heart valves [4]. It was observed that 51.2% of patients with the St. Jude Medical® Mechanical Heart Valve had compensated anemia, though less than 1% of patients were symptomatic. This device was first used in 1977 [5] though, and modern designs have improved upon it, but a persistent problem through all iterations of the valve prothesis: they cause hemolysis.

Roughly 2.5% of Americans have a valvular heart disease (VHD), though this number increases to 13% when examining people over seventy years of age [6]. Some of these patients

can be treated with valve repair surgery, one study suggested that this is about 12% of the patient population [7], but most will need valve replacement surgery. In most cases, this is an open-heart procedure and considered a major surgery.

The history of the mechanical valve prosthesis begins with the Starr-Edwards valve, a caged ball valve developed in the 1950s. An example of one can be seen in Figure 1.1. The Starr-Edwards valve is named for its creators, the surgeon Albert Starr and the engineer Lowell Edwards [8] working in conjunction to solve a problem in the same way that many teams following them would to develop better prosthetics. One such achievement was the St. Jude valve mentioned above, which is shown in Figure 1.2. The Starr-Edwards valve, while functional, placed a large object directly in the path of the blood flow. Patients with a Starr-Edwards valve needed anti-coagulants and blood thinners to prevent clotting. The Starr-Edwards valve was found to produce more hemolysis than the alternative fascia lata graft technique in the presence of valve regurgitation, blood flowing backward through the valve, but was also found to subject the blood to stresses even without the presence of regurgitation [9]. This finding has led to many studies on the effects of prosthetic valves on hemolysis, ranging from studies showing that mechanical trauma associated with heart valves can lower the average lifespan of an RBC from 120 days to 99 [10] to studies indicating that the orientation of the leaflets in a bileaflet valve relative to the aortic wall play a significant factor in the overall hemolysis observed [11]. There are studies covering the valves themselves, but the related problem of paravalvular leakage (PVL) and regurgitation is less well defined.

Figure 1.1: The Starr-Edwards valve was the first widespread artificial heart valve, and is still sometimes used today. [8]

Figure 1.2: A St. Jude Bileaflet Valve. [12]

On a surface wound, a patient may be told to lie still so that they do not “tear their stiches out.” The medical name for this phenomenon is dehiscence, and on a surface wound the treatment is to simply reapply the suture. The valve replacement surgery also requires suture. The artificial housing of the valve, often attached to a mesh fabric called a surgical skirt, must be attached to the cardiac muscle in such a way that it remains secure, even through the comparative trauma that is a constant heartbeat. The solution is suture, which allows a surgeon to tie the artificial tissue, one that would never integrate properly otherwise, to the body and make it functional while doing so. Should dehiscence occur there, around the outer edge of the surgical skirt, it would require another major surgery to correct it, which is often more dangerous for the patients than the resulting condition is. A figure showing the artificial valve in place, along with dehiscence and the resulting paravalvular leakage, can be found in Figure 1.3 below.

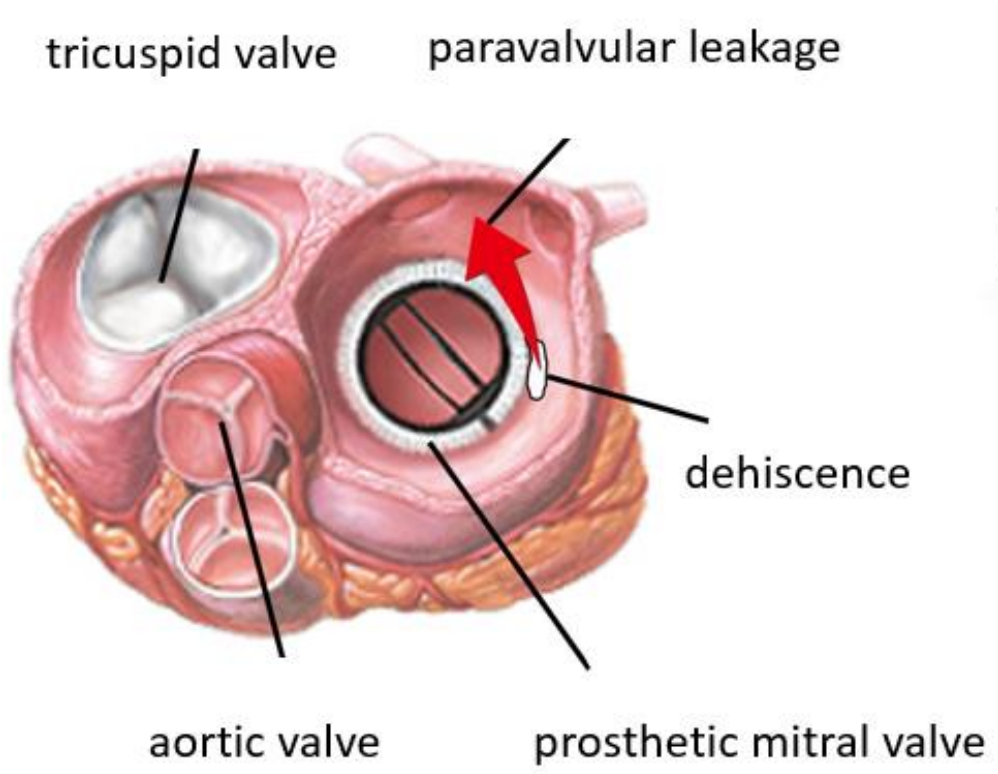

Figure 1.3: A diagram of the interior of the heart, showing three of the valves, two of which are the original biological valves, and one is a mechanical replacement. Adjacent to the replacement is a white region where dehiscence has occurred, and an arrow representing the backflow of PVL. [13]

While there have been some treatments for the symptoms caused by paravalvular leakage shown to be effective in certain cases that do not require surgery, such as oral ingestion of β-adrenergic blockers [10] [14-16], it is still the recommendation of the European Society of Cardiology [17] that paravalvular leakage be corrected surgically. However, the surgical risk for this second operation is roughly 10% greater than that of the original operation [18], and even if the patient survives with no complications, there is no guarantee that the problem will not reemerge again. A proper repair of the PVL is more likely to stay healed than a full valve replacement [19], but continued hemolysis becomes increasingly likely as more surgeries are performed on the same valve [20]. All of this makes surgery a less than ideal solution, even if it

is the most generally effective method to prevent paravalvular leakage and associated mechanical hemolysis. Between 13-42% of all re-operations on the mitral valve are done to address suture dehiscence [21]. There have been some efforts to create an effective percutaneous solution [22], but this solution is time-consuming and technically difficult, while still having only mixed results.

All these solutions aim to correct the problem of hemolysis, and though free hemoglobin is toxic, some amount of it is tolerable. With better understanding of the relationship between paravalvular leakage and hemolysis, physicians would be able to better tailor care to individual patients, recommending surgery to those that need it, but recommending that the problem simply be allowed to persist for those whom surgery would pose too much of a risk. To be clear, that is a minority of the patients. Mortality in cases of conservative therapy is 26%, while it is just 12% for with surgical intervention [23].

Section 1.2: Paravalvular Leakage

There are two major causes of paravalvular leakage. The first is bacterial endocarditis, in which a heart infection has deteriorated the cardiac muscle. The second cause, and the one of greater significance for this study, is due to the deterioration of the seal between the prosthetic ring and the heart wall. A kind of surgical skirt surrounds the prosthetic, and it is this skirt that is typically used to secure the new valve into the heart. As time passes, this skirt is liable to deteriorate, which can lead to paravalvular leakage. The incidence of paravalvular leakage in patients that have undergone heart valve replacement is roughly 7% [24] discounting those patients that coincidentally also had bacterial endocarditis.

Physically, the increased hemolysis occurs because the dehiscence allows a channel to form that is not regulated by the heart valve, and therefore allows blood flow backward through

the heart, which is the specific definition of paravalvular leakage. This narrow channel and reversed flow, or regurgitation, are well documented, but their impact on hemolysis is not. An image of the resulting jet from paravalvular leakage taken via a transesophageal ultrasound is shown in Figure 1.4, and an image showing the channel itself can be found in Figure 1.5.

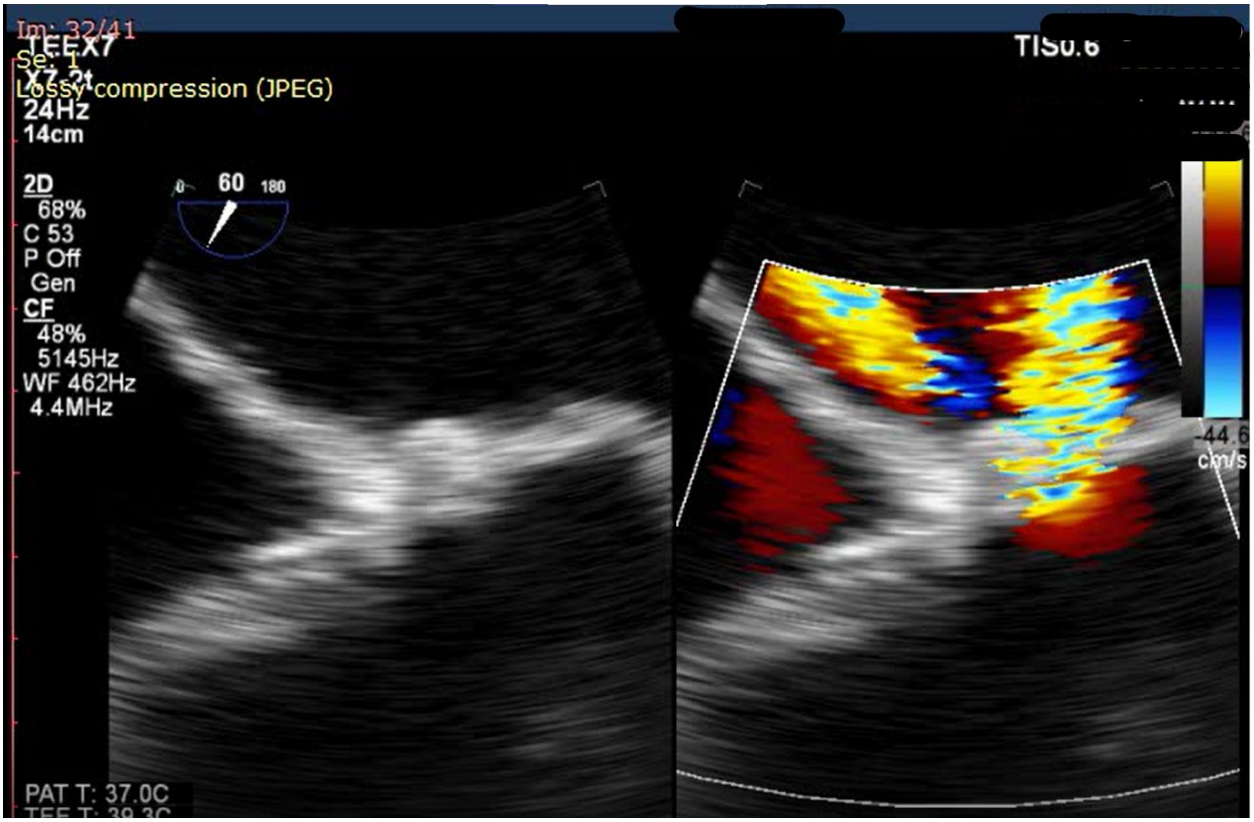

Figure 1.4: A pair of images taken from an animated set of transesophageal ultrasound images. The left image shows the barrier between the atrium and ventricle. The right shows the jetting flow of blood backward from the left ventricle to the left atrium. (Photo has been modified to protect patient confidentiality.) [13]

Figure 1.5: The marked area is thought to be the small channel which allows blood flow from the left ventricle into the left atrium. (Photo has been modified to protect patient confidentiality.) [13]

Figure 1.4 illustrates several important basic facts regarding this research. First, the blood flow from the left ventricle (lower) to the left atrium (upper) proves that paravalvular leakage does occur in some patients, providing part of the motivation for this research. Second, this blood flow has a distinct jetting character, indicated by the roughly cylindrical shape that slowly grows to encompass more area as it travels from the atrial wall. Third, the mixed pattern of yellows and blues shows that though flow is generally in the upward direction, significant mixing is also occurring, which lends credence to the idea of turbulent flow being the appropriate model for this situation.

Madukauwa-David et. al studied the structure of the mitral valve to measure the suture pullout force at differing radial positions [25]. Though they found a trend toward more force

being required to break a suture in the anterior segment of the mitral valve, it was statistically insignificant. Stiles, Kernen, and Stiles found that in general the posterior leaflet is the problem area [26], which is consistent with that trend.

While the existence of paravalvular leakage and its correspondence with hemolysis and anemia were already well known, a quantitative assessment of just how much damage was caused by regurgitation did not exist. Blood is a complex fluid with several possible viscosity models depending on the flow field in question. Rheological models for blood and relevant computational equations can be found in Chapter 2. This work aims to be the first such work to quantify the relationship between paravalvular leakage, turbulence, and hemolysis, in order to help better inform physicians' decisions regarding patient health when this problem is identified. The left atrium is asymmetric, and since there is no radial position where paravalvular leakage is more definite to occur, this asymmetry may play a role in the overall hemolysis. To account for this asymmetry, it was necessary to design a reasonable model of a human left atrium that was both detailed enough to capture this inherent asymmetry while also being generic enough to work as an approximation for the general patient and simple enough to be used in CFD without exorbitant computational resource consumption. The development of this model can be found in Chapter 3, and several less effective though potentially useful methods can be found in Appendix 1. Chapter 4 describes how eddy analysis was implemented, and the results of applying that method to two distinct geometries. Chapter 5 details the conclusions of this study and offers some potential topics for future research in this area.

The problem of dehiscence and subsequent PVL is a significant one, a problem that is most often solved with a surgical correction. This is a good thing; these surgeries save the lives of the patients that undergo them. However, surgery is also a dangerous undertaking, and some

of the patients may not survive that taxing experience, especially since it is likely to be the second or more such taxing experience in a relatively short period of time. Work done in this field, in an attempt to model hemolysis as a function of turbulent flow in biological situations, helps the medical community better understand the complex processes involved. In so doing, physicians are given stronger tools to better recommend surgery to only those individuals who need it and are similarly given the tools to recommend other courses of treatment to those for whom surgery is too great a risk. The ultimate goal of this research, and other projects to follow in this vein, is to better empower doctors with the knowledge they need to treat patients.

2. Blood Rheology and Computational Equations

Section 2.1: Blood Rheology

Given that hemolysis occurs when RBCs are subject to shear stresses, as is the case in microangiopathic anemia, it is imperative to quantify a relationship between turbulence and hemolysis. Before this can be accomplished, it is necessary to find an appropriate rheological model for blood viscosity. Blood can be modeled as a generalized Newtonian fluid, as according to Equation 1:

$$\tau = \eta(\dot{\gamma})\dot{\gamma} \qquad \text{Equation 1}$$

Here, τ is the shear stress, η is the apparent viscosity, and $\dot{\gamma}$ is the shear rate [27]. For very high flow rates, modeling blood as a Newtonian fluid is unlikely to introduce significant error [27]. However, since the flow rate in this biological system is unknown and variable, it would be inappropriate to assume a Newtonian model. In fact, some early preliminary work assuming a Newtonian model showed that the large volume of the atrium coupled with the relatively small pressure gap between the inlet and outlet led a large region where the shear rate on blood was quite small. The Newtonian model cannot account for the aggregation of RBCs, a phenomenon that occurs with high frequency in blood subjected to low shear rates. An alternative model is that of a Bingham plastic, modelled by Equation 2:

$$\dot{\gamma} = \begin{cases} 0, & \tau < \tau_0 \\ \dfrac{(\tau - \tau_0)}{\eta}, & \tau \geq \tau_0 \end{cases} \qquad \text{Equation 2}$$

Where τ_0 is the yield stress. The Bingham plastic model is not often used for blood, but it is illustrative of the concept of the yield stress. When the stress is less than the yield stress, RBCs

have a tendency to agglomerate into stacks called rouleaux (singular, rouleau), which causes plug flow instead of normal fluid flow [28]. This model can be used over small values of shear the shear rate, but fails to account for the continued breakup of rouleaux, which is a gradual process. As higher shear rates are reached, the remaining rouleaux become smaller, which continues to contribute to the overall viscosity. Over a large range of shear rates then, it is necessary to account for this shear-thinning behavior. An image of one of these rouleau, a French word meaning "roll" and intended to evoke images of coins stacked atop each other, can be seen in Figure 2.1 below.

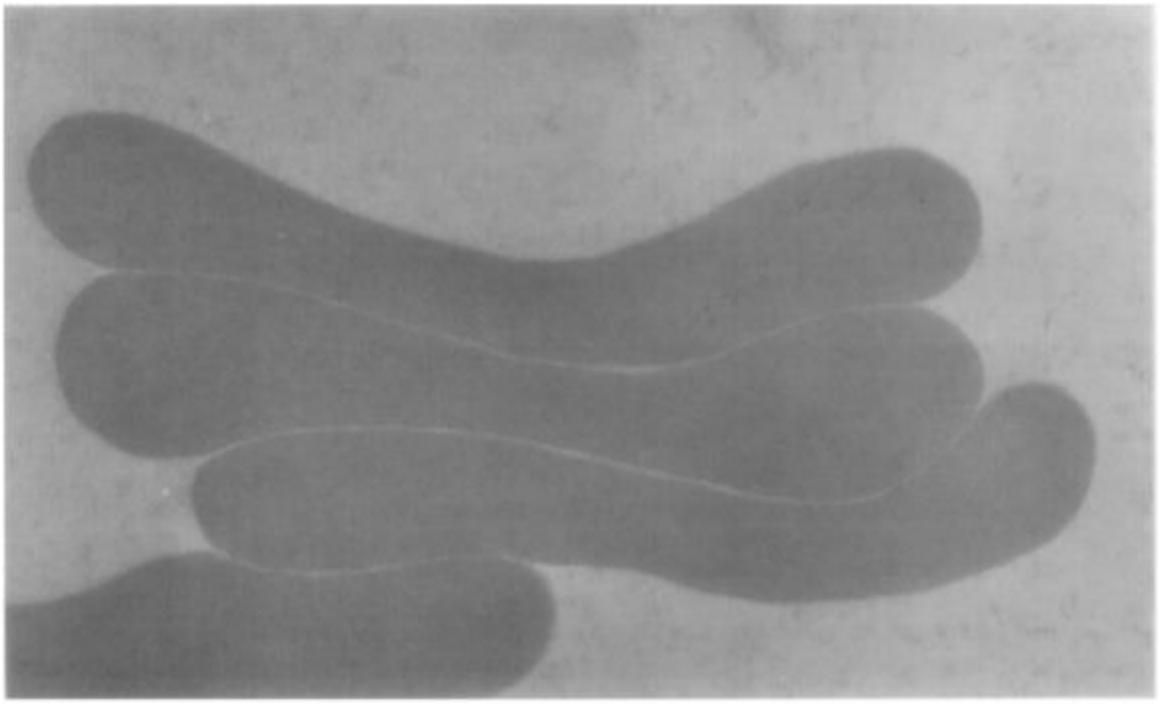

Figure 2.1: A transmission electron microscope image of four RBCs (side view) that have stacked on top of each other to form a rouleau. [29]

One model that has been proven effective for modeling blood was first introduced by Casson to model pigments in paint [27]. Blood and paint are similar in that both are colloidal suspensions in which the particulates tend to agglomerate, and so Casson's model has been applied routinely to blood flow for 60 years. It is given by Equation 3:

$$\sqrt{\tau} = \sqrt{\tau_0} + \sqrt{\eta * \dot{\gamma}} \qquad \text{Equation 3}$$

This model both preserves the Bingham plastic characteristic of yield stress and introduces a shear thinning component, and while not as accurate as newer models based on the microstructures of the RBCs [30], it is easier and less resource intensive to implement into a computational fluid dynamics (CFD) environment.

A model thus established, it is possible to relate the shear stress to a measure of hemolysis known as the hemolysis index (HI). For this purpose, the model proposed by Leverett [31], as shown in Equation 4, has traditionally been used.

$$HI = C\ \tau^{\alpha} t^{\beta} \qquad \text{Equation 4}$$

where C, α, and β are empirical model parameters, τ is the shear stress as defined in Equation 3, and t is the exposure time of the RBCs to that shear stress. This model works fairly well for laminar flows in which the shear stress and the exposure time are both fairly regular, but for turbulent flows in which both of these values can vary across both time and spatial dimensions, the model is difficult to apply accurately. The empirical constants were developed using laminar flow experiments, and therefore do not consider the variability inherent in turbulent flow. Recently, work has been done to better model the HI in turbulent flow regimes by Ozturk [32]. Ozturk examined the results of the classical experiments done by Forstrom [33], Sutera and Mehrjardi [34], and Kameneva et. al [35]. Those experiments give the geometry and measured hemolysis of a jet, a Couette viscometer, and a capillary tube, respectively. Operating under the theory that eddies of Kolmogorov Length Scales (KLS) roughly on the same size as RBCs are most likely to cause significant hemolysis, Ozturk prepared in silico environments that aptly

recreated the conditions of the classical studies. She then simulated the flow fields of those experiments with the express goal of designing an equation that could be generally used in all turbulent flow conditions to correlate the KLS of the eddies in that turbulence with the hemolysis that they cause. That work produced Equations 5 and 6.

$$HI = a + bt + cEA_{KLS(0-3)} + dEA_{KLS(4-6)} + eEA_{KLS(7-9)} \quad \text{Equation 5}$$

$$HI = bt + cEA_{KLS(0-4)} + dEA_{KLS(5-7)} + eEA_{KLS(8-10)} \quad \text{Equation 6}$$

Here, there are five empirical model parameters, a, b, c, d, and e, and t has the same meaning it does in Equation 4. Note that the empirical constants for Equation 5 are not the same as those for Equation 6, and all the constants can be found in Table 2.1. While they are very different in form, Equations 5 and 6 do reflect some of the same parameters that can be found in Equation 4. All three equations rely on empirical constants, and do not follow from fundamental biology. The exposure time of Equation 4 is reflected in the exposure time term in Equations 5 and 6, though the inclusion of the surface area of the eddies also influences the amount of time RBCs are exposed to stress. The KLS values are a corollary to the shear stress term in Equation 4, as both parameters that aim to quantify the stress RBCs undergo as they are subjected to flow conditions.

Table 2.1: Empirical Constants for Equations 5 and 6

	a	b (s^{-1})	c (m^{-2})	d (m^{-2})	e (m^{-2})

Equation 5	1.62e-7	1.82e-7	3.08e-5	3.42e-6	1.72e-6
Equation 6		5.57e-4	2.45e-5	2.67e-6	1.14e-6

EA stands for Eddy Area, and the subscripts are used to describe the size range of the eddies that fall into that group. The size is found from the Kolmogorov Length Scale in μm as a result of CFD simulations and is defined by Equation 7.

$$KLS = \left(\frac{\nu^3}{\varepsilon}\right)^{\frac{1}{4}} \quad \text{Equation 7}$$

Where ν is the kinematic viscosity and ε is the energy dissipation rate per unit mass. The Kolmogorov Length Scale is derived from the theory that all turbulent flows behave similarly when examining the size of the eddies that make them up. Those eddies are affected by the kinematic viscosity of the fluid and the rate at which energy is transferred, causing large eddies to break up into smaller ones. Simple dimensional analysis reveals the only mathematical way to combine those two parameters and have the result be a length is Equation 7. A similar technique led to the creation of the Kolmogorov Time Scale and Kolmogorov Velocity Scale, which often have relevancy to similar projects as the KLS does but are not used in this project.

Ozturk's equations are not perfect. They include four and five empirical constants which have dimensions. These dimensions do not have any physical implications but are necessary because the terms on the right-hand side of the equation are dimensioned, while the HI itself is dimensionless. Because of this, Equations 5 and 6 can only be used in the units specified in the table, which somewhat limits the scope. However, in absence of a more fundamental model for understanding turbulence and its relationship to hemolysis, the empirical model has been shown by Ozturk to be reasonably accurate over a variety of flow conditions.

Also included in Ozturk's work is the technique of eddy analysis, in which the flow field volume of interest is broken into many cross-sectional areas, and the amount and size of the various eddies represented in that cross section are measured. The findings are then averaged with those of the next cross section to estimate the behavior of the volume in between. This approach leads to errors in averaging, but provides a way to measure the surface area of eddies, which is not a feature the CFD program of choice, ANSYS Fluent [36], allows. The surface area of the eddies of each appropriate size is totaled across the entire volume of interest, and that serves as the values for Equation 5.

Section 2.2: Computational Equations

A k-ω SST viscosity model was used with the default parameters in Fluent 19.1. This turbulence model has been shown to be effective in previous work for similar situations [32] [37]. The k-ω SST model is a combination model, importing some elements of the Wilcox k-ω and the k-ε models [38]. The k-ω model is well suited for turbulent flow in the viscous layer, while the k-ε model is most useful for regions far from the wall. Using a combination of both ensures that the flow is well modelled throughout the flow field. The governing equations behind k-ω SST viscosity are given as Equations 8 and 9 below.

$$\frac{\partial}{\partial t}(\rho k) + \frac{\partial}{\partial x_j}(\rho k U_j) = \frac{\partial}{\partial x_j}\left[\left(\mu + \frac{\mu_t}{\sigma_k}\right)\frac{\partial k}{\partial x_j}\right] + G_k - Y_k \qquad \text{Equation 8}$$

$$\frac{\partial}{\partial t}(\rho \omega) + \frac{\partial}{\partial x_j}(\rho \omega U_j) = \frac{\partial}{\partial x_j}\left[\left(\mu + \frac{\mu_t}{\sigma_\omega}\right)\frac{\partial \omega}{\partial x_j}\right] + G_\omega - Y_\omega + D_\omega \qquad \text{Equation 9}$$

In general, these two equations are intended to allow the CFD program to solve for k, the turbulent kinetic energy, and ω which is ε/k, where ε is the turbulent kinetic energy dissipation rate, which also appears in the definition of the KLS. In these equations, μ is the viscosity, μ_t is

the turbulent viscosity, σ_k is the turbulent Prandtl number for k, G_k is a generation term for k due to mean velocity gradients, Y_k is the dissipation of k due to turbulence, σ_ω is the turbulent Prandtl number for ω, G_ω is the generation term for ω, Y_ω is the dissipation of ω, and D_ω is the cross diffusion term [38]. Mathematical expressions for the generation, dissipation, and cross diffusion terms may be found in the user's manual for Fluent [38].

3. Developing an Atrial and Dehiscence Slit Model

Section 3.1: Model Development

For the purpose of approximating the hemolysis, it is most convenient to use CFD to model blood flow through a model paravalvular leakage. ANSYS Fluent 19.1 [36] was the software program selected. Before using the CFD to solve the flow problems, first a model of the mitral valve and left atrium was necessary.

The first thought was to recreate the structure of the heart from digital medical images taken of it by using CAD packages. This proved to be a difficult endeavor, as the images available for public use were usually too far apart to detail the atrial structure properly, and the tools sets provided in ANSYS Design Modeler [39], the integrated CAD program with Fluent are not ideal for the task. This solution was abandoned in favor of adapting a ready-made 3-D printing file to fit the purposes of this research. Many months were spent on trying to adapt this file, removing extraneous structures, converting between file types, and above all else trying to fix the thousands of individual problems that prevented it from meshing, including overlapping faces, faces with poor aspect ratios, and nonplanar faces. Full descriptions of several automated methods to fix these problems can be found in Appendix A, in addition to more detailed

descriptions of the issues surrounding building a model in Design Modeler, but this method was additionally abandoned after the sheer number of unacceptable geometric properties proved to be too labor intensive to be worthwhile.

These failed approaches led to a final, successful approach. To create the three dimensional atrium model, 44 image slices were obtained that showed the pericardium wall at differing depths in the atrium [40]. In combination with these images, the software "Free-D" developed by Andrey and Maurin [41], which specializes in combining cross sections at differing depths of a 3D object into a reasonable 3D model was implemented. Because of computational limits within Fluent, only every other image was used when constructing this model. The model resulting from Free-D can be found in Figure 3.1

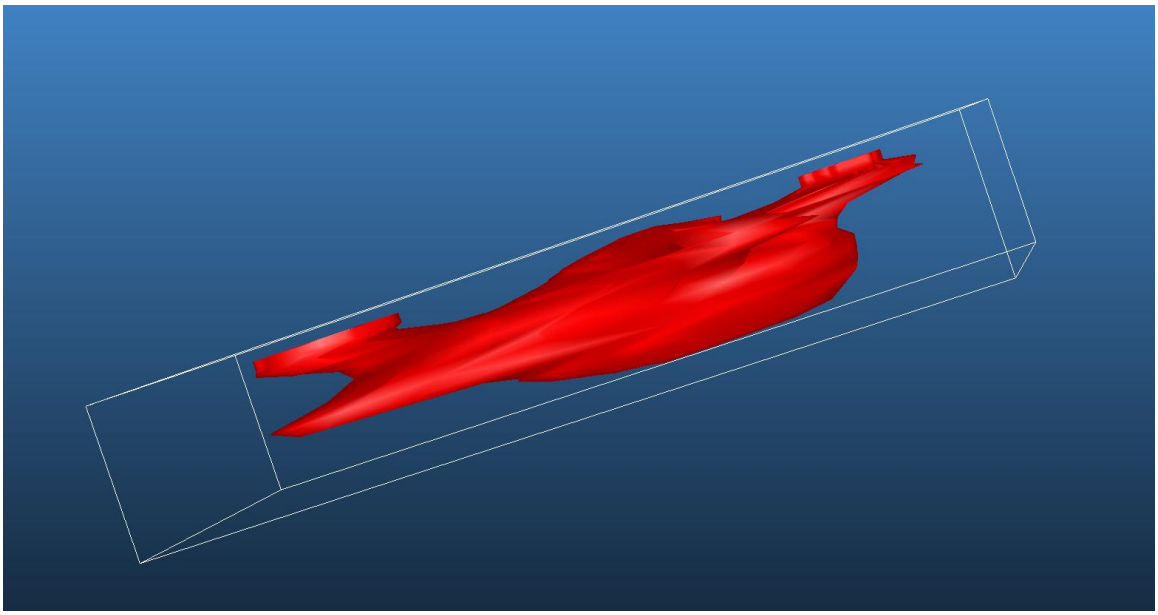

Figure 3.1: The model of the left atrium as obtained from Free-D. Both the top and bottom of this model, where the final and first cross-sections are respectively, are not sealed.

The model editing software Blender [42] and the CAD program attached to Fluent, Ansys SpaceClaim, were used to touch up the model, including sealing the openings that were left in the shape of the first and the final cross section on the top and bottom of the model, reducing the

prevalence of the pulmonary veins, adding an approximation of the St. Jude valve structure, and inserting a semi-cylindrical channel 1 mm in diameter and 3mm long along the edge of the valve structure in an arbitrary radial position to represent the defect caused by dehiscence. It was one initial goal of this research to test if the location of this channel impacted the hemolysis observed by altering its position, though the results from this initial arbitrary position showed this to be unnecessary.

These dimensions are based on the estimation of a physician who has experience working in this field [13] and some guidelines as to how to best accomplish the surgery [43], but both the structure and dimensions are an estimation only. First, like any biological phenomenon, it is unlikely that paravalvular leakage occurs in exactly the same way in any two different people. The shape of this channel is therefore patient specific, and the postulated structure of dehiscence presented here may vary wildly on an individual basis. Second, this estimate was drawn from observing hearts at a specific moment in time. The constant cardiac motion is also very capable of causing deformation of this channel, including closing it completely at differing points in the heartbeat. The way blood behaves *in vivo* could vary substantially from what is observed after death. That said, correcting for these two deficiencies is not trivial. The first would require an individual patient to model, and the second would require a better moment-to-moment understanding of the deformation of the PVL channel. Lacking these pieces of information, the assumptions made regarding the shape of the channel are thought to be the most appropriate for a general use case, even acknowledging that they could be improved upon.

The Ansys meshing program was used to mesh the model for CFD calculations. Of the several meshing methods available as options, only the cartesian method produced a viable mesh. All other methods encountered fatal errors with the geometry that caused them to be

unable to mesh all or part of the model. The result was a mesh consisting of 1,572,766 tetrahedral cells, 140,958 exterior faces, 3,079,527 internal faces, 4 large outlet zones where the pulmonary veins lead to the atrium in normal flow, and a single tiny inlet zone consisting of just 30 faces at the top of the paravalvular leakage channel. The inlet and broader mesh can be found in Figures 3.2 and 3.3 below. Additionally, a second model was constructed with an approximation of a suture fiber still within the channel at an arbitrary position, as though the suture had come undone with some of the thread still hanging inside of it. This opening is shown in Figure 3.4.

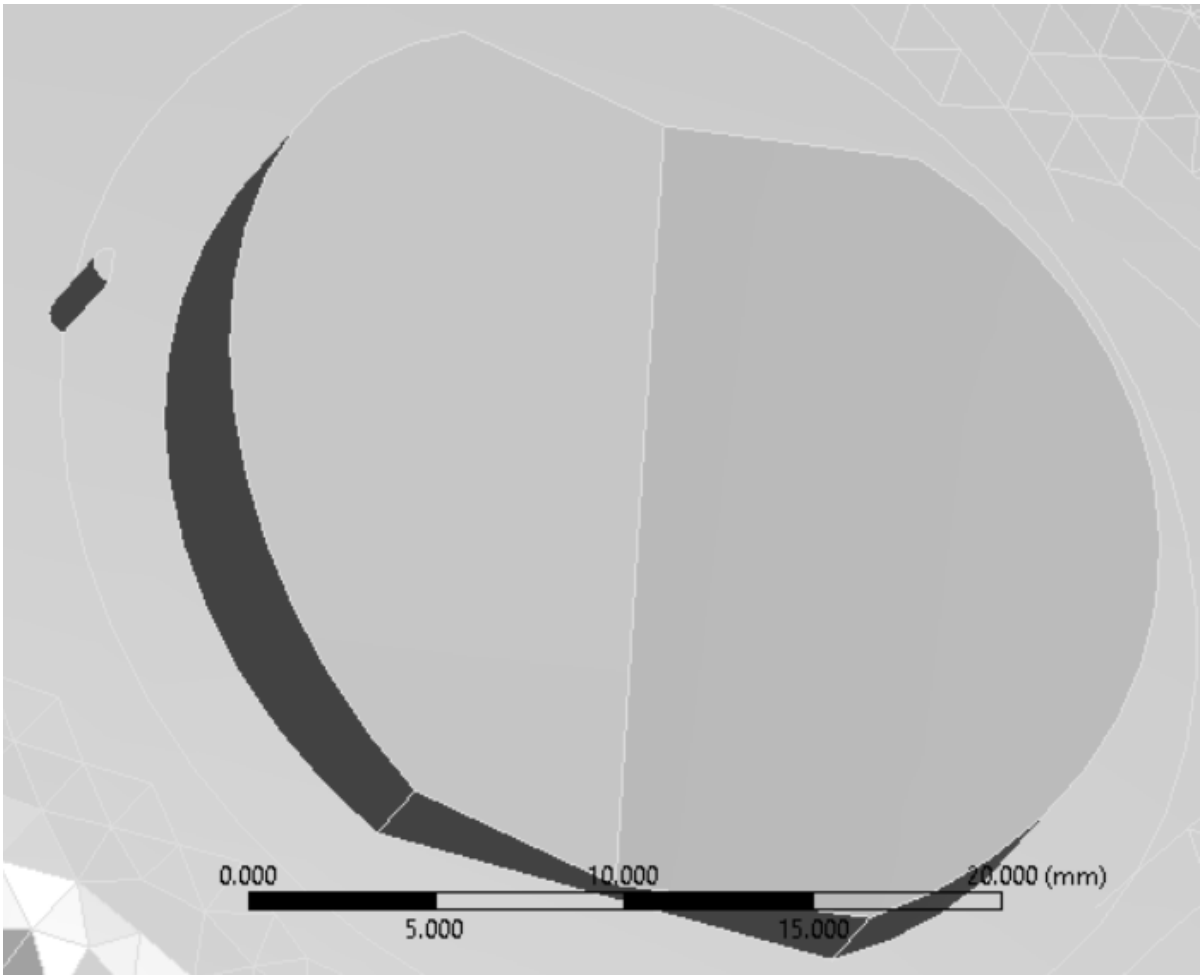

Figure 3.2: A close-up of the paravalvular leakage channel and flow inlet, pictured here as a semi-cylinder next to the larger valve structure. The larger structure that they rest on is the left atrium, and the camera would be positioned somewhere within the left ventricle.

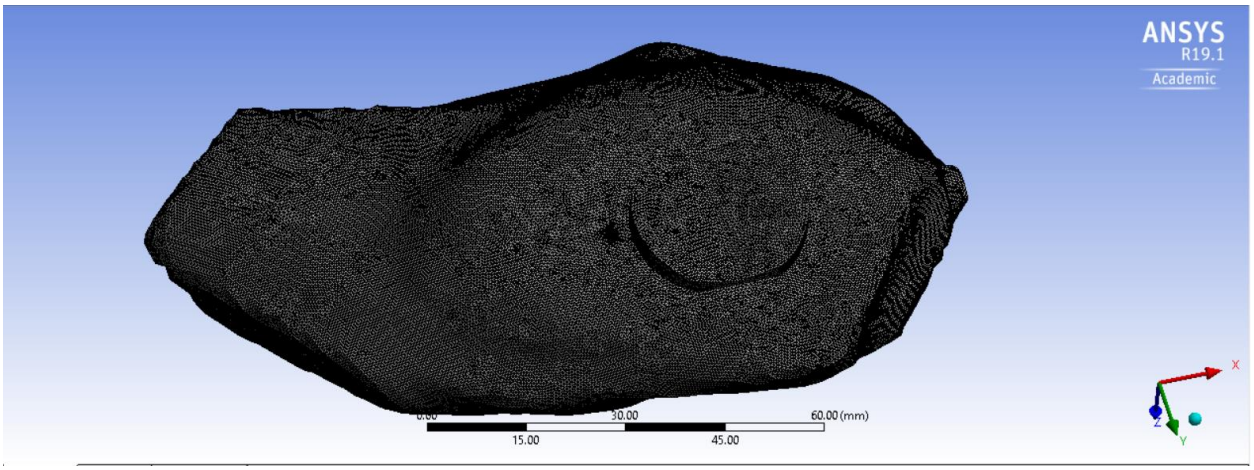

Figure 3.3: A wide angle view of the whole model from the same angle as Figure 2.2. The channel and valve structure both appear in the center, and the four truncated pulmonary veins are also visible.

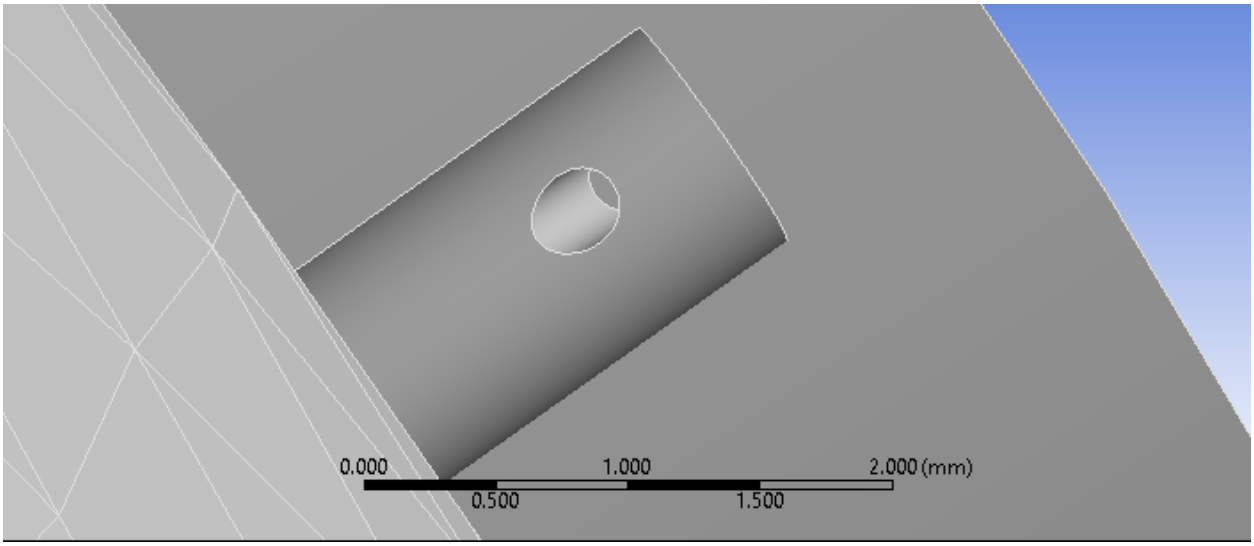

Figure 3.4: A close-up view of the hole representing the leftover suture wire.

Regarding the dimensions of the suture, there are some assumptions involved. The positioning and angle are arbitrary, but beyond that there is some guess work as to the size of the suture involved. Table 3.1 shows the most common suture sizes.

Table 3.1: The sizes of various common sutures.

USP size		minimum (mm)	maximum (mm)	Tension (N)
12-0	Thin	0.001	0.009	—
11-0		0.010	0.019	—
10-0		0.020	0.029	0.24
9-0		0.030	0.039	0.49
8-0		0.040	0.049	0.69
7-0		0.050	0.069	1.37
6-0		0.070	0.099	2.45
5-0		0.100	0.149	6.67
4-0		0.150	0.199	9.32
3-0		0.200	0.249	17.4
2-0		0.300	0.339	26.3
0	Thick	0.350	0.399	38.2
1		0.400	0.499	49.8
2		0.500	0.599	62.3
3-4		0.600	0.699	71.5
5		0.700	0.799	—

USP stands for United States Pharmacopeia and is how doctors typically reference the size of a suture, not with the numerical value of that suture's diameter. Originally, technological limitations meant that a size 1 suture was the smallest, but as filament manufacturing technique improved, a suture with a smaller diameter was produced, which was called a size 0 suture. Eventually, that fiber too was upstaged by a smaller fiber, and rather than numbering that suture in the negatives, or shifting the whole list and causing massive confusion, that suture was labelled a double 0, or 2-0. The modern scale goes up to 12-0. The suture used in the model was a 2-0 suture, which is typical for this kind of surgery [44], though variations do exist.

Section 3.2: Verification

To verify the grid independence of this model, an alternate mesh was created that used a smaller maximum side length for the tetrahedrons, going from 0.3 mm to 0.2 mm. Doing this massively increased computational time, requiring more than a week of ongoing computation for the residuals to drop below 10^{-4}, and even destabilized the program in some instances, leading to crashes and more lost time. For these reasons, the 0.3 mm mesh was highly preferential, as though simulations still required between 48 and 96 hours, Fluent was less likely to crash upon loading the mesh. A comparison of the centerline velocities of the jet from the 0.5 mm mesh and the 0.4 mm mesh can be found in Figure 3.5 below. The two do differ slightly in some areas but are thought to be reasonably close enough that the additional computational complexity is not worthwhile.

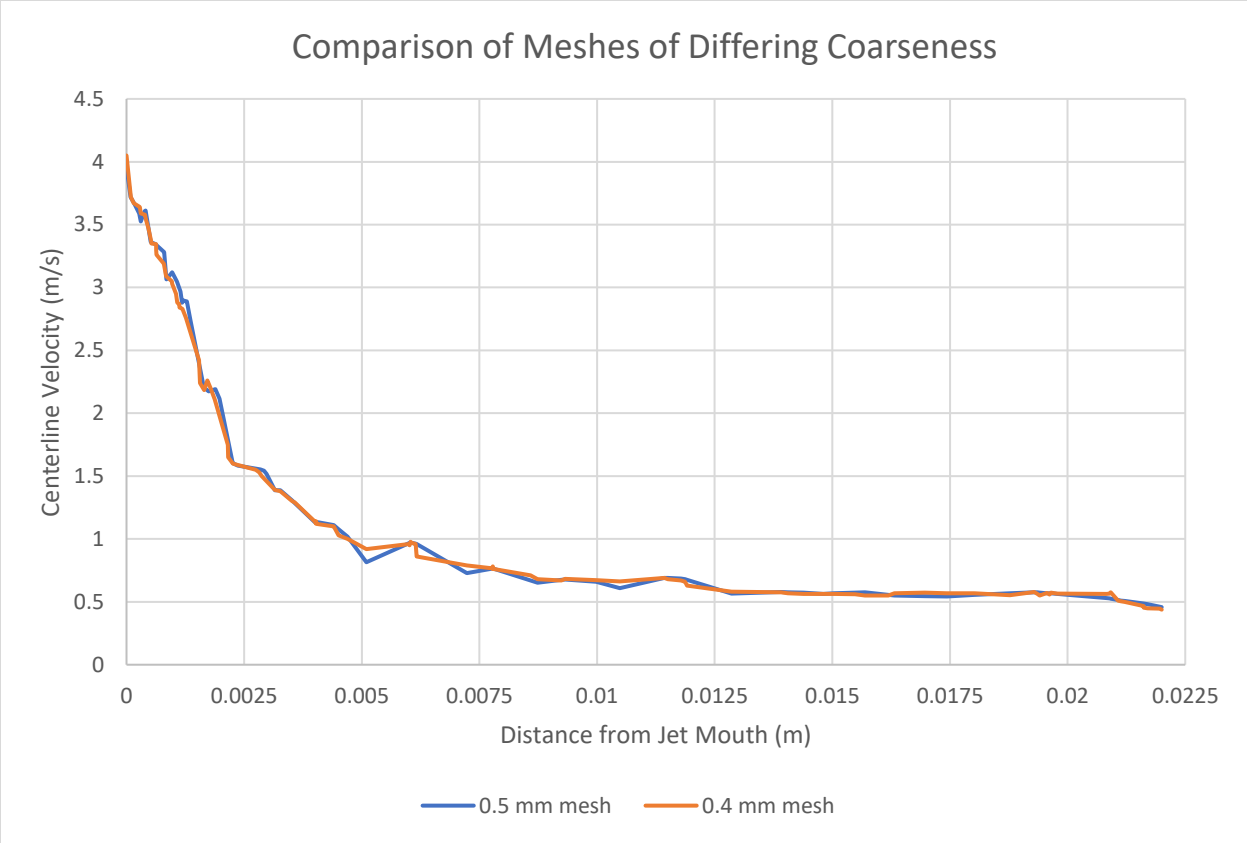

Figure 3.5: A comparison of the centerline velocity of the jet across two different possible meshes. The orange line represents a finer mesh, and though there is some disagreement and the orange line is generally smoother, the difference is not enough to justify the additional computational resources required to use the finer mesh.

Additionally, The Mark/Adapt Cells feature of Fluent was used to further refine volumes where the velocity changed quickly. This feature allows the user to automatically mark cells that fall outside a certain boundary in a parameter. In this case, it was used on cells where the velocity was found to change by more than 0.1 mm/s. These marked cells are then adapted. In this case, that means being refined by being broken down into smaller pieces, though it is possible to coarsen the mesh if there are volumes where very little change is occurring. This tool was used in order to ensure that all parts of the mesh were appropriately sensitive to changes in the flow pattern. This tool cannot fully replace refining the mesh as a whole, but it does ensure that the most relevant portions are fully refined, and its use is an indication that the eventual mesh was not a factor in the results.

Blood was modeled as a fluid of constant density 1060 kg/m^3, and a user defined function for viscosity consistent with the Casson model. For the purposes of this experiment, $\tau_0 = 0.041$ dyn/cm^2, and $\eta = 0.029$ dyn/cm^2, though both these values are dependent on the hematocrit and fibrinogen levels of the blood [27], and could vary somewhat from patient to patient. This user-defined function was verified by solving the velocity profile of the Casson model for a cylindrical pipe analytically. This analytical solution was then compared to a simulated pipe and the two solutions showed good agreement. These two velocity profiles can be seen together in Figure 3.6. For more information regarding this user defined function, see Appendix 2.

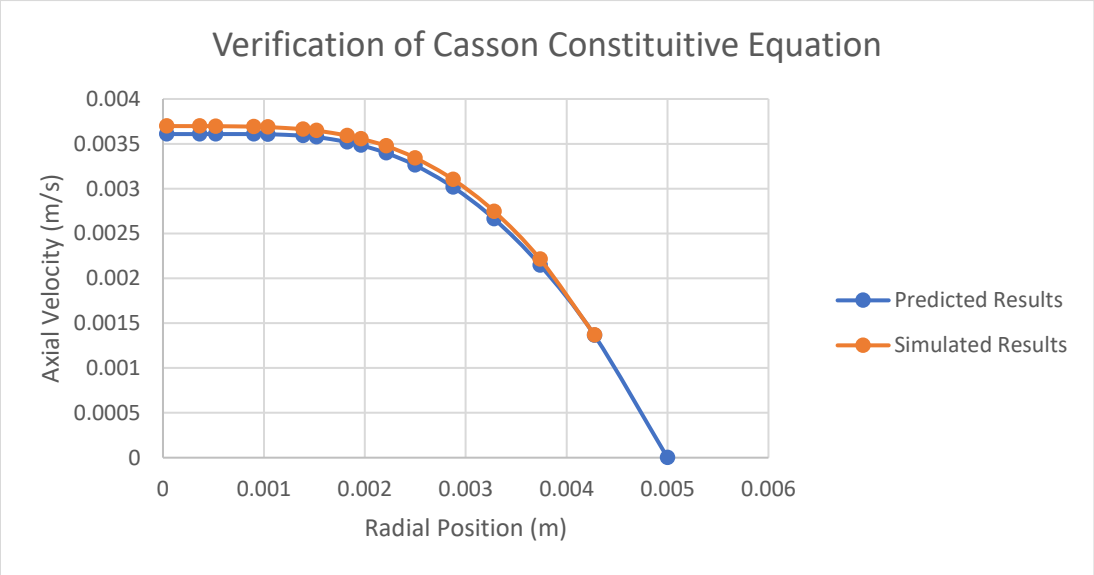

Figure 3.6: Comparison of theoretical and simulated velocity profiles.

Section 3.3: Simulation Parameters

The inlet was set to a pressure inlet, and was given a set pressure of 18,000 Pa, which is roughly 135 mmHg. Depending on the guideline and the physician, this sets the patient just above or just below the hypertensive range [45-46]. Each of the four exits was set to a pressure outlet at 1,300 Pa (10 mmHg) [47]. The SIMPLE solution scheme was chosen in accordance to previous work [37] [32].

The solution was considered converged when each of the continuity, x-velocity, y-velocity, z-velocity, k, and omega residuals were less than 10^{-4}. The under-relaxation factors can be found in Table 3.2. These under-relaxation factors were slowly lowered to these eventual values from their defaults as the simulation failed to converge even given over 72 hours of simulation time. Lowering these values increases the time per iteration but can lead to better convergence.

Table 3.2: The Under-Relaxation Factors

Property	Default Value	Final Value
Pressure	0.3	0.1
Density	1	0.1
Body Forces	1	0.1
Momentum	0.7	0.1
Turbulent Kinetic Energy	0.8	0.05
Specific Dissipation Rate	0.8	0.05
Turbulent Viscosity	1	0.05

4. Results and Discussion

Section 4.1: Velocity and Pressure Analysis

The first thing analyzed upon the completion of the simulation was the velocity profile, both because it was relatively simple to create and understand, but also because the results were expected. As predicted, the velocity profile showed a jet with a relatively high velocity channel and inlet, followed by a large amount of space where there was little flow. This velocity profile is shown in Figure 4.1.

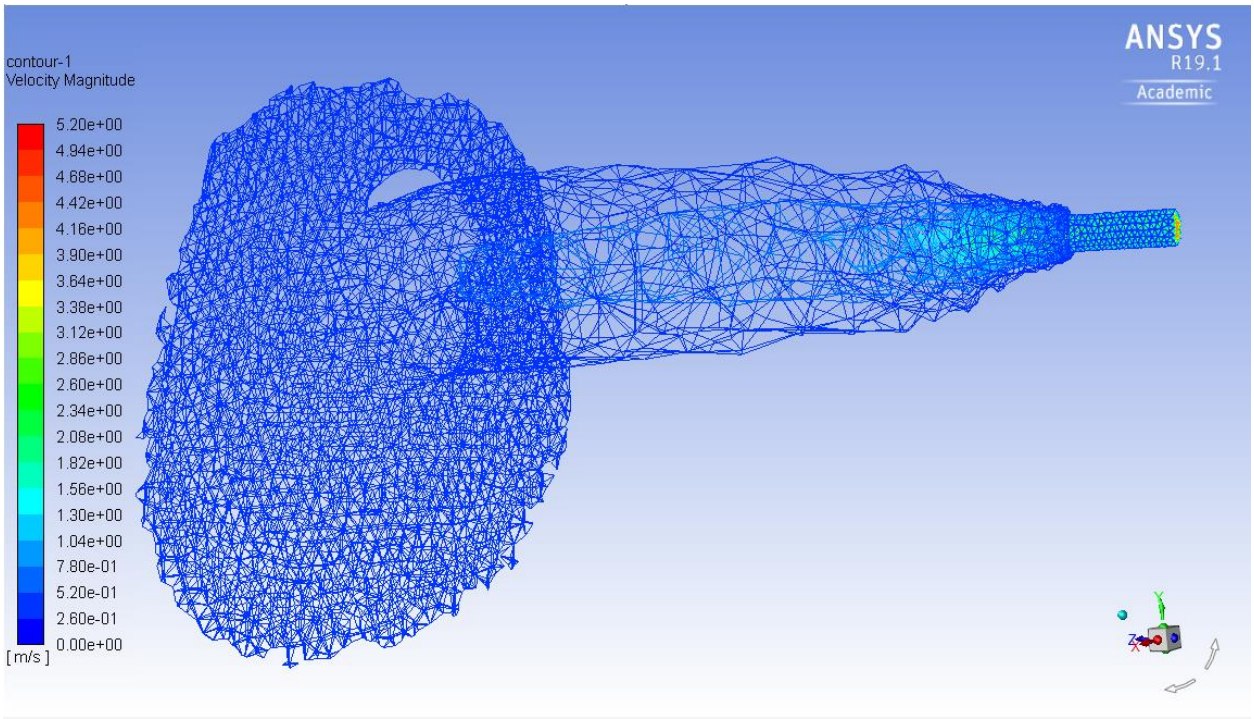

Figure 4.1: The velocity profile of the blood flow within the atrium. The inlet channel is on the right and is the only place where the higher velocity volumes are located. The blood then emerges via jet and continues flowing until it hots the far wall of the atrium. Most of the volume has blood flowing so slowly that it does not appear in this graphic.

Most of the atrium volume has too little flow to be shown using the velocity scale of Figure 4.1, which is not unexpected. This simulation is continuous, but the loss of momentum still accounts for the very slow flow rate through most of the area. Figure 4.2 gives a close-up view of the jet as it immediately leaves the channel, as described by several layers of the velocity

profile spaced 0.5 mm apart. This diagram helps to illustrate how quickly the flow both slows down once it enters open space, and how quickly the jet area expands. Figure 4.3 shows the first of these planes, at the edge of the channel, compared to the sixth plane 2.5 mm deeper into the atrium. Figure 4.2 shows that the jet is not quite perfectly circular in cross section. Instead, it has an ellipsoid shape, presumably because the opening into the atrium is not perfectly circular. The half-circle opening causes a flattened circular jet, which is especially evident at cross secions closer to the mouth of the jet. As flow is allowed to progress further, it takes on a more perfectly circular shape. Because of this non-circular shape, it is impossible for the jet to be truly axis-symmetric, but the jet is roughly symmetrical about the line of symmetry of the mouth. In these 2.5 mm represented by Figure 4.2, the maximum centerline velocity decreases from 4 to 1.5 m/s, a rather extreme deceleration that explains why the regions of extreme turbulence can only be found within the PVL channel. Figure 4.4 shows that the final centerline velocity is around 0.5 m/s, a velocity that close to constant at the point where the jet impacts with the wall of the atrium, roughly 15 mm after first entering the atrium. Because of the turbulent nature of the flow within the channel, the exact centerpoint of the jet is not necessarily the point with the highest velocity. Figure 4.3 shows the velocity of each point on the plane coincident with the mouth of the jet, and that of the plane 2.5 mm deeper into the atrium. The velocity is viewed on the y-axis, and the numerical position along the x-axis of the model is the x-axis of Figure 4.3. Flow is generally in the z-direction. The red and white peaks are not along the same x position, indicating that the centerline of the jet may not account for the highest velocity present at any given cross-section of the jet. Regardless, Figure 4.3 does show that the maximum velocity is more than halved in those 2.5 mm, while the radius of the jet doubles.

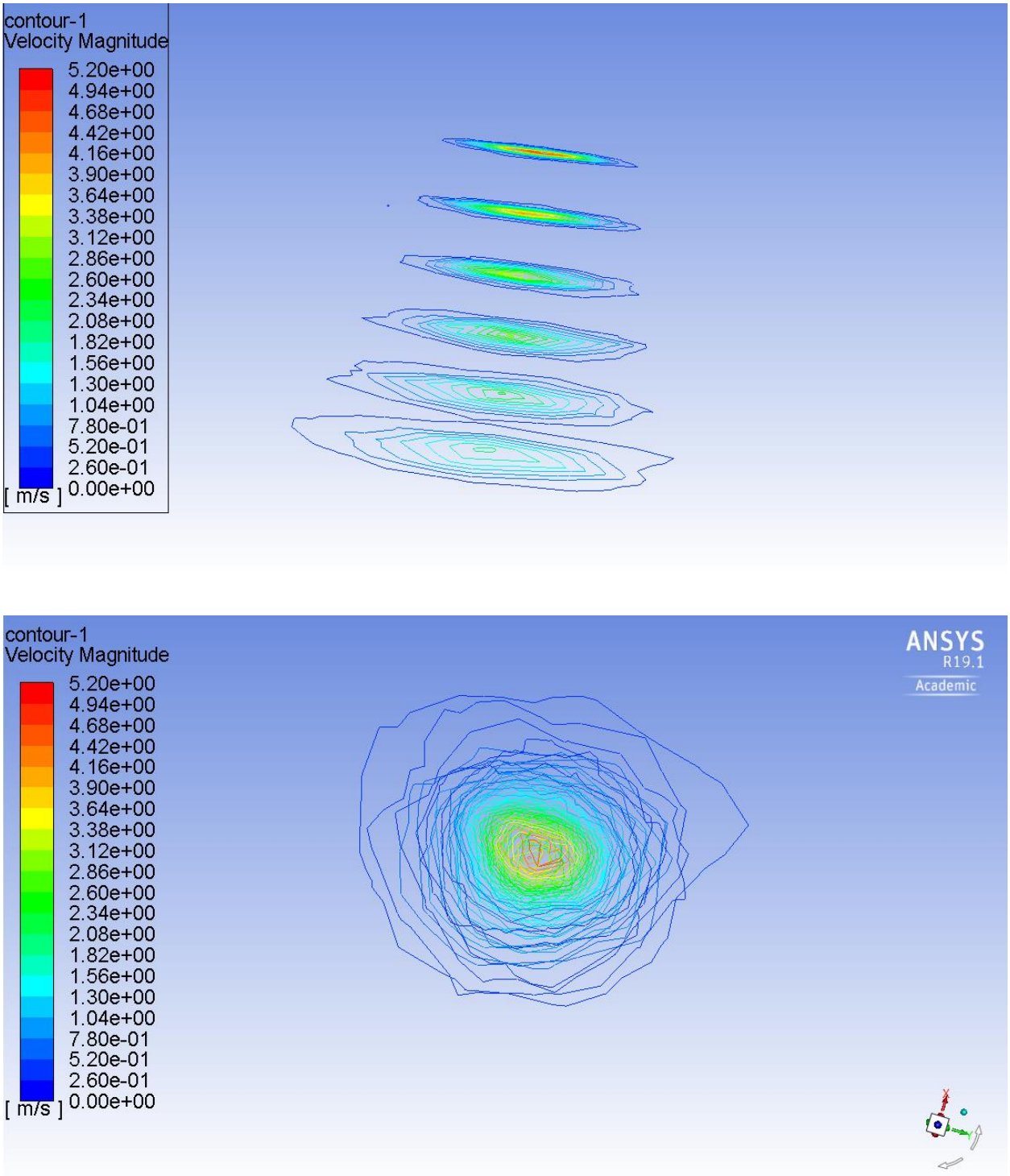

Figure 4.2: A series of six velocity profiles of the jet starting just at the mouth of the channel as it enters the atrium proper, and the next 2.5 mm down. The same set of six profiles is shown from a side view (top) and a top down view (bottom). The top image better shows the change in magnitude at the center line, and the bottom image shows the expansion of the jet as it moves.

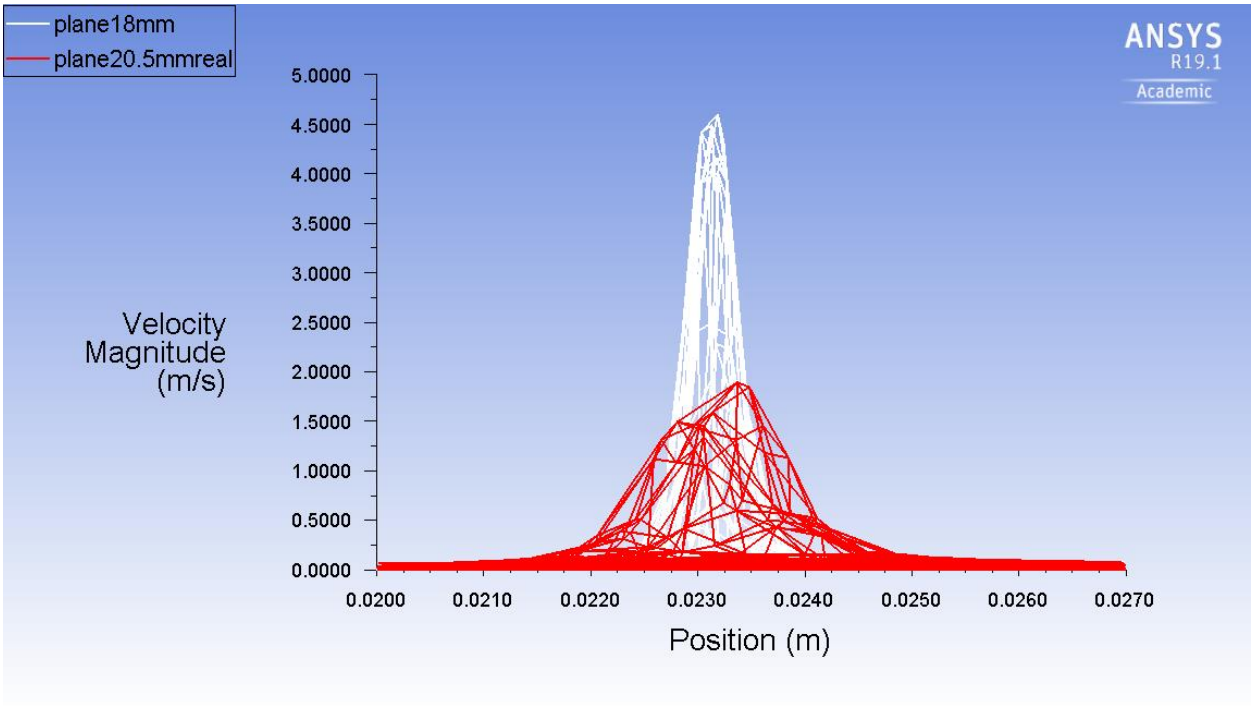

Figure 4.3: In white is the velocity profile of the plane at the edge of the PVL channel. Its central velocity magnitude is more than double that of the central velocity of the jet just 2.5 mm into the atrium (red), and at that point the diameter of the jet had doubled.

Figure 4.4 shows the maximum velocity in the z direction, into the atrium, as a function of the distance travelled from the PVL channel. It shows a steady and sharp decline followed by

a gentle levelling off.

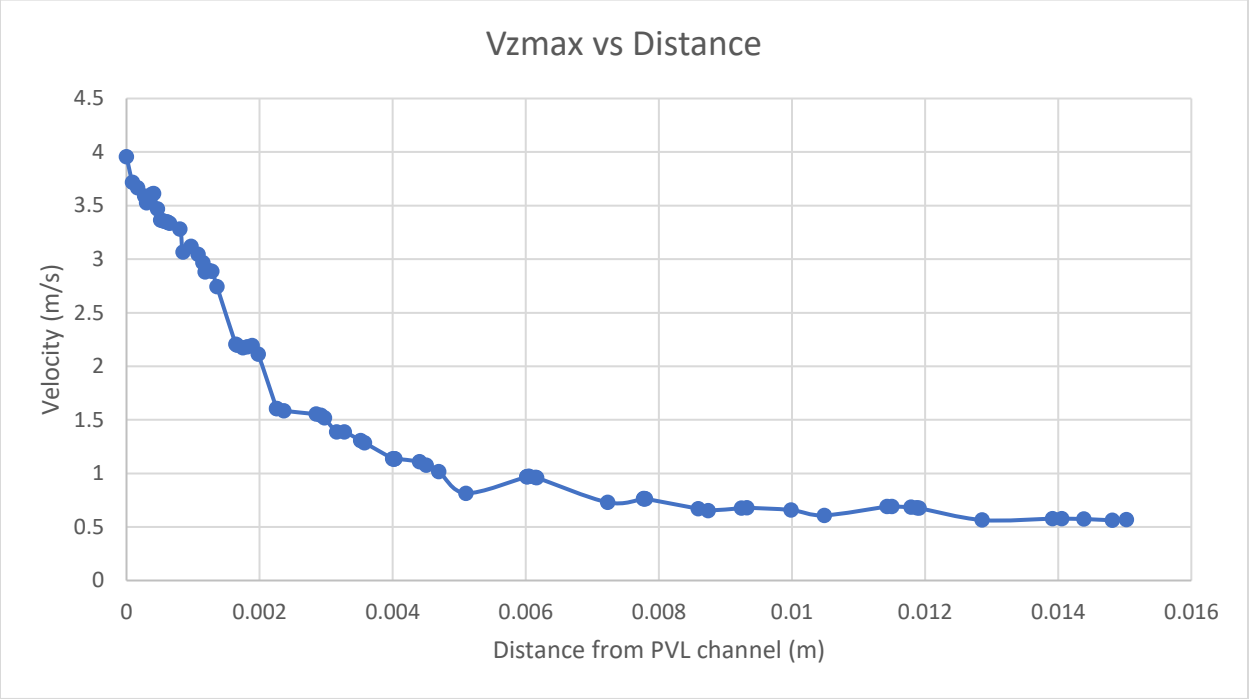

Figure 4.4: The centerline velocity of the jet as a function of distance from the opening into the atrium where the jet begins.

The total pressure drop across the whole model is 127 mmHg, or about 17 kPa. The pressure drop across just the PVL channel is approximately 7.5 kPa. A graphical representation of this can be found in Figure 4.5.

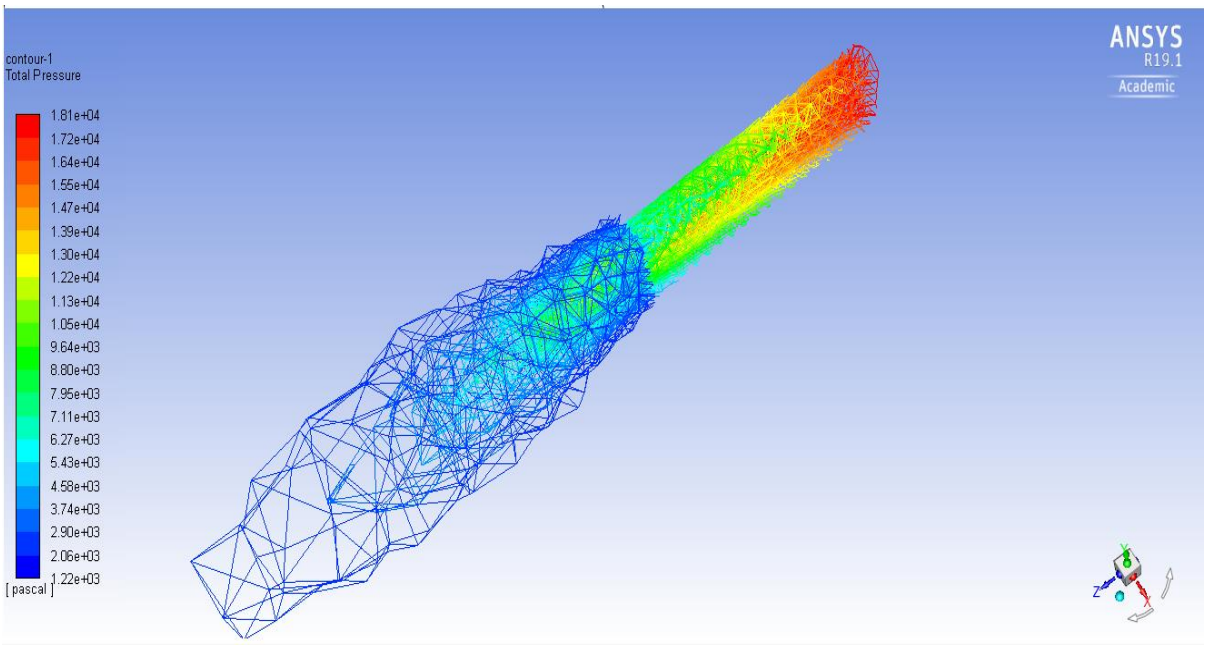

Figure 4.5: The pressure drop across the model. The rest of the empty space within the atrium has fluid in it, and therefore has some pressure, but it is not enough to appear on this scale, which has a minimum value of 1,200 Pa.

Figure 4.5 shows that the majority of the pressure drop occurs within and very close to the PVL channel. At the mouth of the channel, the central pressure is approximately 10.5 kPa, and roughly 3 mm further into the atrium, the total pressure has become so small everywhere that it does not register on this graphic's scale, which has a minimum value at 1,200 Pa. Figure 4.6 shows the pressure along the centerline of the jet, similar to how Figure 4.4 shows the velocity along this centerline. This Figure 4.6 has less detail than Figure 4.5, and thus may be easier to read but less informative, while still providing an idea of the same general information. The pressure drops dramatically across the first 3 mm after exiting the PVL channel, and then levels off to a very stable level shortly after that. The leftmost point on the x-axis represents the point on the model at which fluid exits the PVL channel and enters the atrial structure proper. The rightmost point with data displayed is the wall.

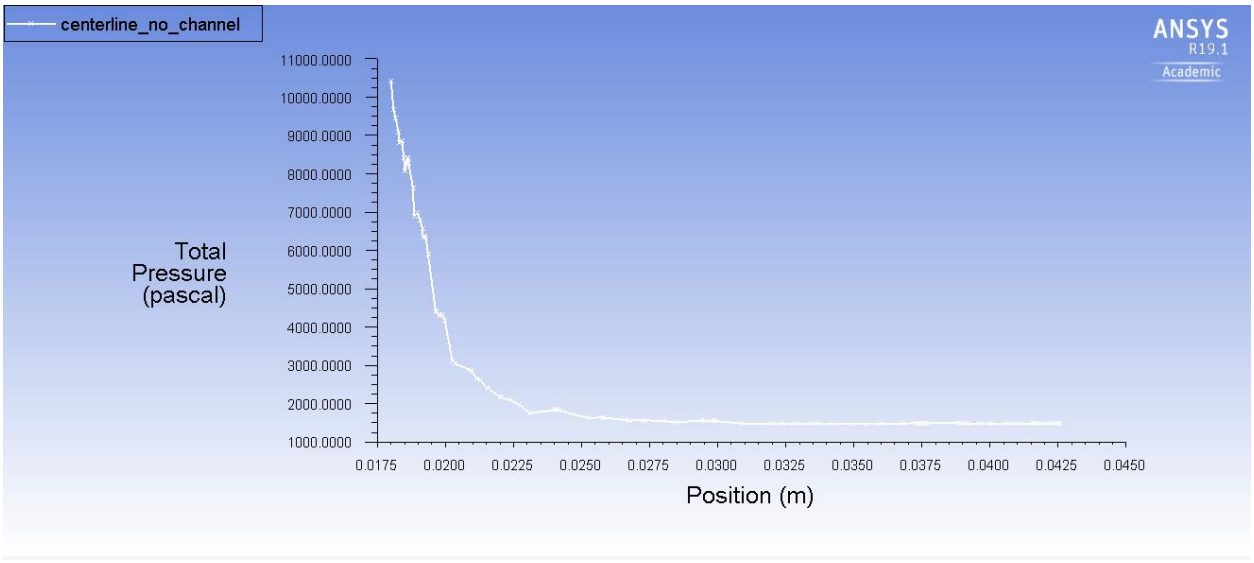

Figure 4.6: The centerline pressure drop of the jet as a function of distance from the mouth of the PVL channel. By 5 mm past the mouth of the channel, there is almost no pressure drop through the rest of the volume.

Section 3.2: Turbulence Analysis

Figure 4.7 shows a heat map of the areas where the KLS of the eddies is in the critical 1-10 µm range. The 0-1 µm range is also important per Ozturk's eddy analysis method but is not represented in these calculations because no such areas existed in the simulated results.

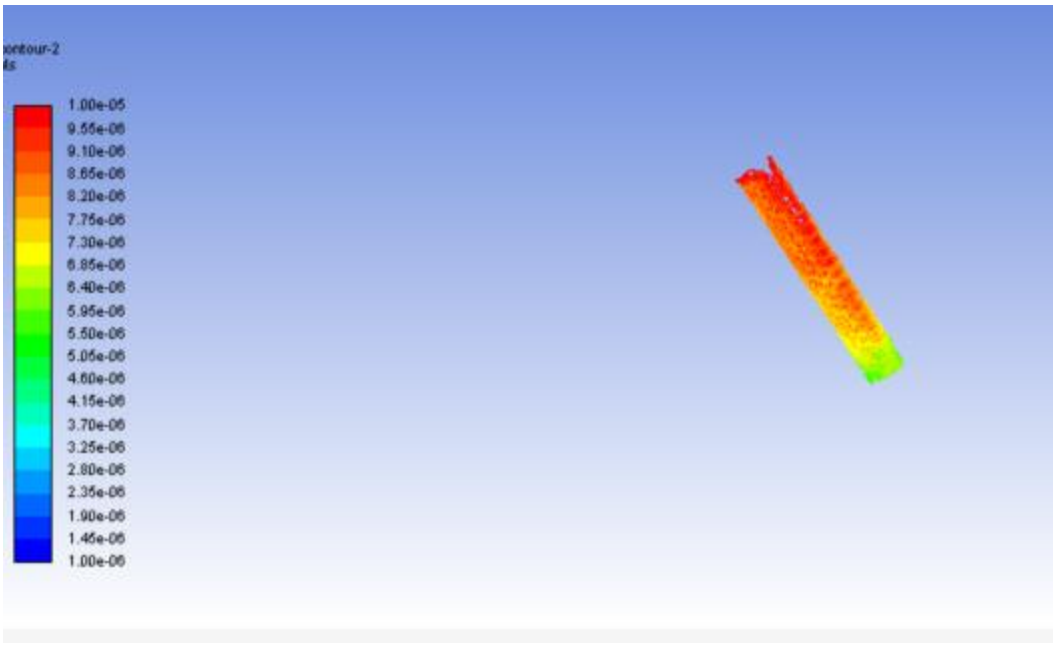

Figure 4.7: Shows the only locations where the size of the turbulent eddies is similar in magnitude to the size of individual RBCs. If the eddy is significantly larger than the RBC, then the cell will be caught in the flow, but not necessarily damaged by it.

Figure 4.7 is a highly magnified view of only the inlet channel, with the green end representing the ventricle side, and the red end representing the atrium side. It was upon discovering this that one of the questions initially envisioned for this project was answered, and the project modified. Originally, the radial location of this channel was thought to impact the overall hemolysis, but since the volume of the atrium does not contribute to hemolysis, the radial location of the slit is irrelevant.

Eddy analysis was performed on this result. Fluent allows the user to create planes a set distance away from, but perpendicular to, an existing plane. In this case, seven planes were created at 0.5 cm intervals descending from the inlet. These seven planes covered the extent of the area containing KLS values of the appropriate range. Fluent also allows for the creation of iso-clips: surfaces on other surfaces that only fall in the specified range for a specified parameter. Here, each of the seven planes was used to create iso-clips for KLS values between 0-1 µm, 1-2 µm etc., up through 10-11µm. this would normally result in 77 iso-clips, but only 26 were non-

zero. A surface integral was taken for each of these clips to determine the area represented by eddies of appropriate KLS on the original seven planes. This gives accurate values at each of the planes.

To determine the behavior of the flow in the intervening space between the planes, the average for a given KLS value was taken between the top and bottom plane. This average was then translated into a volume by multiplying by the distance between the planes. The surface area and volume of eddies of sizes ranging from 0.5 μm to 10.5 μm are then calculated assuming the eddies are perfect spheres. The total volume taken up by a given class of eddy is then divided by the total volume each eddy consumes, resulting in a total number of eddies, which can then easily be multiplied by the surface area of each eddy to find a total surface area. These total surface areas are then summed in the buckets suggested by Equations 5 and 6. For the exposure time, an arbitrary resting heart rate of 60 beats per minute, or 1 second per beat. The percent difference between using 60 bpm and 100 bpm is 0.01%, so the choice is largely irrelevant and can vary greatly by patient. Table 4.1 Shows the results of this analysis.

Table 4.1: The Results of the Suture Free Model

	KLS 0-3 or 0-4 (m^2)	KLS 4-6 or 5-7 (m^2)	KLS 7-9 or 8-10 (m^2)	HI
Equation 5	0	39,000	520,000	1.02
Equation 6	0	160,000	520,000	1.02

A similar process was followed for the model with a piece of suture remaining in it. This suture was modelled after a 2-0 monofilament suture, which has a diameter of 0.3 mm as shown in Table 3.1 above. It's modelled as a cylinder that intersects the defect created by the dehiscence at an arbitrary angle. That heat map is shown in Figure 4.8, and the results of the eddy analysis are shown in Table 4.2.

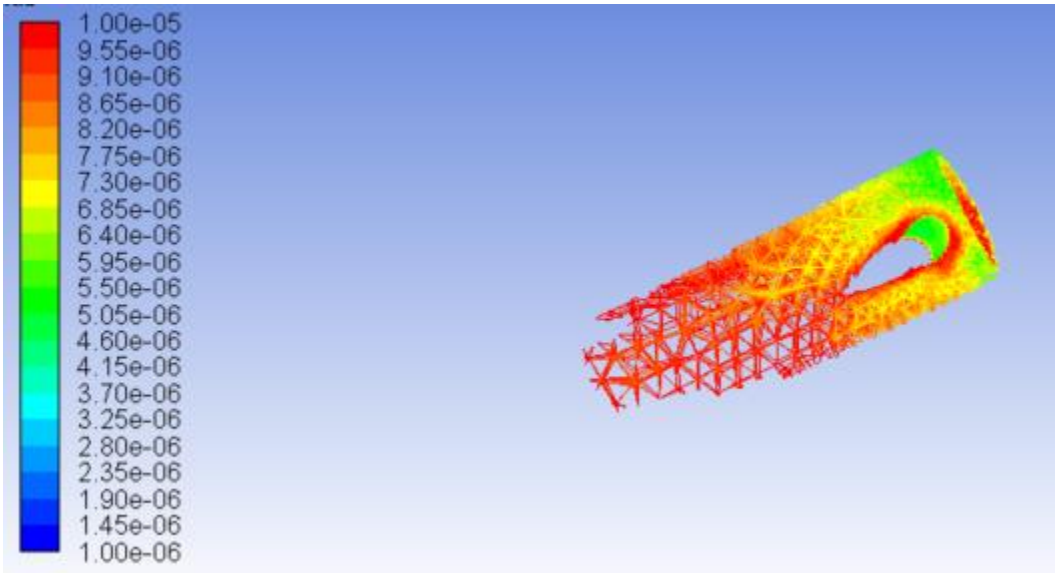

Figure 4.8: A zoomed in heat map of the channel with a bit of suture wire still hanging in the passageway. This leads to a smaller total volume taken up by eddies, but the volume that is used is more intensely turbulent.

Table 4.2: The Results of the Suture Included Model

	KLS 0-3 or 0-4	KLS 4-6 or 5-7	KLS 7-9 or 8-10	HI
Equation 5	0	73,000	500,000	1.11
Equation 6	2,000	210,000	480,000	1.16

If an average value for hemolysis is taken for each model, the first model yields an average of 1.02 and the second an average of 1.135, which is approximately 11% higher. The HI can be read as a percentage of the RBCs expected to be hemolyzed by passing through the

turbulent flow. If just over 1% of the blood in a human body were hemolyzed with every heartbeat, this issue would be a major catastrophe, but reading the results this way would be out of context. This is a very small slit that opens at the same moment the aorta, the largest blood vessel in the body, opens. For reference, the cross-sectional area of this slit as modelled, which could vary slightly, is approximately 0.4 mm^2. The aortic opening is 506.7 mm^2 on average, which is 1250 times larger. If the amount of blood that exits the ventricle with each beat is proportional to these openings, then only 0.08% of the blood in each beat is hemolyzed.

The average left ventricle has a maximum blood volume of 142 mL at diastole and 47 mL at systole. This gives the average volume of blood per beat to be 95 mL. Of these, it is expected that 0.07 mL will pass through the dehiscence, and that 0.0007 mL will be hemolyzed per second. The half-life of hemoglobin is about 0.27 hours [48]. This gives a decay constant of $7.2*10^{-4}$ seconds. Equation 8 shows the relationship between the amount of a decaying substance remaining, N, after time, t, has passed, with initial amount of substance, N_o, and the decay constant λ.

$$N = N_0 e^{-\lambda t} \qquad \text{Equation 8}$$

Using an iterative solution in which N_o in each iteration is equal to N from the previous iteration plus the 0.0007 mL, a steady state value is eventually found to be 1.03 mL of hemolyzed blood. For the average human adult, 5 L of total blood is a common approximation, which gives a free hemoglobin concentration of $2.06*10^{-4}$, assuming no suture is present, or 1.15 mL at steady state for a concentration of $2.3*10^{-4}$ with the suture. These concentrations, assuming that the average person has roughly 15 g/dL of hemoglobin [2], lead to a plasma free hemoglobin concentration of 3.09 or 3.45 mg/dL respectively. The normal range in a healthy person can be anywhere from 0-15.2 mg/dL [49], though physicians typically don't diagnose hemolysis until plasma free

hemoglobin reaches 40 mg/dL [50]. Typically, physicians turn to other markers of hemolysis such as the presence of schistocytes, and elevated reticulocyte count, high LDH, low haptoglobin, or high bilirubin, all of which are detectable in tests done on sight in a hospital. The plasma free hemoglobin test generally requires an outside blood lab to do analysis, which is both more expensive and less expedient [50]. A summary of these results can be found in Table 4.3 below.

Table 4.3: A summary of the numerical results both with and without additional blockage left in the flow channel.

Model	HI	Steady-State Hemolyzed blood (ml)	Hemolyzed blood / Whole Blood	Plasma Free Hemoglobin (mg/ dL)
No Blockage	1.02	1.03	$2.06 * 10^{-4}$	3.09
Blockage	1.135	1.15	$2.3*10^{-4}$	3.45

If the average person has roughly 15 g/dL of hemoglobin in their blood, then finding 3 mg/dL of plasma free hemoglobin indicates roughly 0.02% of their blood cells are hemolyzed at any given time. This is consistent with the finding of roughly $2*10^{-4}$ mL of hemolyzed blood per mL of total blood, which is also 0.02%. This falls within the normal expected range of plasma free hemoglobin detected when taking a blood draw from patients, which is between 0-15.2 mg/dL, but is the result of an atypical situation, and so may be added to a test that occurs in a normal range. For instance, if a blood draw were to find a patient with 7 mg/dL of plasma free hemoglobin, it would be impossible to determine if that is a naturally occurring 7 mg/dL or if that result is a combination of a natural 4 mg/dL plus the 3 mg/dL caused by PVL.

5. Conclusions and Future Work

Section 5.1: Conclusions

While the radial position of dehiscence was ultimately found to be irrelevant with this model, some important medical information can be gained from this research. First, sutures present inside dehiscence channels will increase the turbulence within those channels. The addition of a single suture fiber in the dehiscence channel model led to roughly 11% more hemolysis. With an accurate representation, physicians might also gain the knowledge of the free hemoglobin concentration in a patient suffering from this condition and no other major risks for hemolysis, which could help inform their decision making. Correcting dehiscence is another major surgery in a patient already recovering from one, and is therefore risky, costly, and painful. This information may be used to deem the hemolysis an acceptable risk and avoid that second surgery.

The major points to take from this work include:

- All the hemolysis caused by PVL occurs in the channel and not in the larger atrial structure.
- The damage occurring in the channel means the radial position of the channel is largely irrelevant.
- Irregularities in the channel geometry increase the total amount of hemolysis.

Section 5.2: Remaining Questions and Future Work

This work has led to several additional questions on the topic of dehiscence and paravalvular leakage. It was assumed during the course of this investigation that the radial position of the paravalvular leakage, which could occur in any radial position though the posterior would appear to be more common [13], was irrelevant because all of the turbulence

which might cause hemolysis was located within the channel between heart chambers, and not within the atrium itself. This assumption has not been proven, and an additional project examining it might produce new results or help solidify those found within this thesis. Additionally, blood flow is not a continuous process, but rather a cyclical one. The constant flow method used in this analysis is not accurate to how the biological system operates, and an additional experiment in which the cyclical nature of this process was examined could include interesting results. Included among these cyclical changes is the possibility that the channel itself is closed during diastole and only opens in response to increased pressure during systole. This kind of deformable mesh simulation necessarily takes more computing power, so it was deemed extraneous for this first round of experimentation, but a more focused project may find that use of computational resources acceptable.

The results of this experiment are not consistent with the medicine, as the normal range for free hemoglobin in the bloodstream is between 0-15.2 mg/dL, and the simulated results show only an increase of roughly 3-3.5 mg/dL. It is possible that this is because the test for plasma free hemoglobin involves pricking to draw blood, and that said pricking can itself result in hemolysis. While the predicted additional free hemoglobin is within the normal range, the range exists only to account for issues with the testing method. A healthy person or a person with paravalvular leakage may have identical numbers in their plasma free hemoglobin tests, and a medical diagnosis could then only be made if the patient were also exhibiting symptoms of anemia. This study therefore emphasizes the difficulty in detecting and diagnosing paravalvular leakage, even if the absolute magnitude of the predicted hemolysis is within the normal range. However, at least one case study reports that a patient with severe hemolytic anemia had plasma free hemoglobin levels of 87.9 mg/dL [51], which is far beyond what is considered the normal range.

Results like this indicate that the PVL examined in this study is relatively mild, and that additional work is necessary to fully understand the extent of hemolysis.

Hemolysis from paravalvular leakage is a significant problem that sometimes requires additional surgeries to correct, and the amount predicted by this study is inconsistent with that reality. Additional work is needed to correct this incongruity. The most obvious target is the shape of the dehiscence channel. A smaller channel would subject the blood flowing through it to greater turbulence, leading to more hemolysis as a percentage of blood travelling through the channel per beat, but would allow less total blood through. Additionally, the exact method of suture dehiscence may need additional exploration. The way pullout sutures lead to PVL will lead to a different channel geometry than PVL caused by bacterial infection. This thesis does not attempt to model the deterioration of the valve skirt itself, but such a deterioration could lead to defects of significantly different character. The skirt itself may even act like a filter over the mouth of the channel, and the results with the suture still in place indicate that this is likely to cause even greater hemolysis. Such alterations to the channel may provide the missing medical agreement, but additional testing is required. Many of the assumptions made throughout this report are patient specific and will vary from person to person. The size of the mitral valve, the systolic pressure, the total blood volume and volume moved per heartbeat, and the shape of the atrium are all parameters that will not match in most situations, and may or may not be relevant to the overall result. Many additional experiments which alter these parameters could be undertaken in an attempt to predict a result consistent with medical science, or they could all be altered to simulate a specific patient.

The volume of the PVL channel is of particular interest. Consider a theoretical capillary channel, through which only a single RBC could flow at a time. In a channel like this, it would

be impossible to subject more than a single RBC at a time to the stress caused by turbulence, even though the much smaller channel would normally indicate higher velocities and greater turbulence. In this scenario, there would be very little total hemolysis because the volume is so small. Next, consider a theoretical heart where there simply is no wall between the ventricle and the atrium. This heart would not be functional for maintaining life, but because the channel between the ventricle and the atrium is so large, there would be very little turbulence, even as nearly all the blood is subjected to that turbulence. In either of the supposed theoretical cases, the total hemolysis is very low. This would seem to indicate that there is a maximum value of hemolysis which occurs at an unknown defect volume, which occurs when the channel is large enough to allow significant blood flow, but small enough to still cause turbulence. Finding this maximum is one possible future endeavor.

While mitral valve replacement is common, any of the heart's valves may need to be replaced, and in the case of a different valve replacement, a similar yet distinct problem could arise. The new paravalvular leakage in these locations will have many similarities to the mitral paravalvular leakage examined here, yet the differences in pressures and distances between heart chambers and within blood vessels would lead to a unique situation. In these cases, additional experimentation is necessary to determine if there are significant differences.

This work is predicated strongly on Ozturk's eddy analysis methodology. While reasonably accurate, especially for turbulent flow, it is always possible that sometime in the future a more accurate or more robust model will be developed. For instance, her work-related turbulence for experiments in which exposure time varied by 5 orders of magnitude, so additional research might lead to the refining of the coefficients. In that case, and if that model can be applied to a CFD simulation, this work should be revisited with a better and renewed

understanding of blood's fluid dynamics and hemolysis in response to turbulence. This question is still largely unexplored, and more information is expected to follow shortly.

The areas still left unexplored, but that merit future research include:

- Altering the size, shape, angle, location, and regularity of the defect.
- Employing a time-dependent mesh that deforms in accordance with a regular heartbeat.
- Development of a system which can easily be altered to fit individual patient needs.
- Updating the results if a more appropriate link between turbulence and hemolysis is ever developed.

Appendix 1

The first approach to the creation of the heart model was to find images of MRI scans of the entire heart, and piece together different cross sections using the software included in the Fluent package, ANSYS Design Modeler [52]. The images in question came from the Visible Human Project (VHP) produced by the National Library of Medicine (NLM) in under the National Institute of Health (NIH) [53]. There were several problems with this approach. First, to anyone outside the field of medicine, it is difficult to distinguish between different types of tissue in an image like those provided by the VHP. This led to confusion about exactly where the heart muscle wall began and ended, making accuracy difficult to gauge. Second, the distance between available images was thought to be too large for accurate modeling, especially the ends of the model. At the time, it was not known that the majority of hemolysis occurs only in the paravalvular slit, and so creating a fully accurate model of the interior heart chambers was deemed important. Third, Design Modeler has a limitation to splicing between ellipsoids. It will always try to connect the major axes together, leading to situations like those found in Figure A1.1

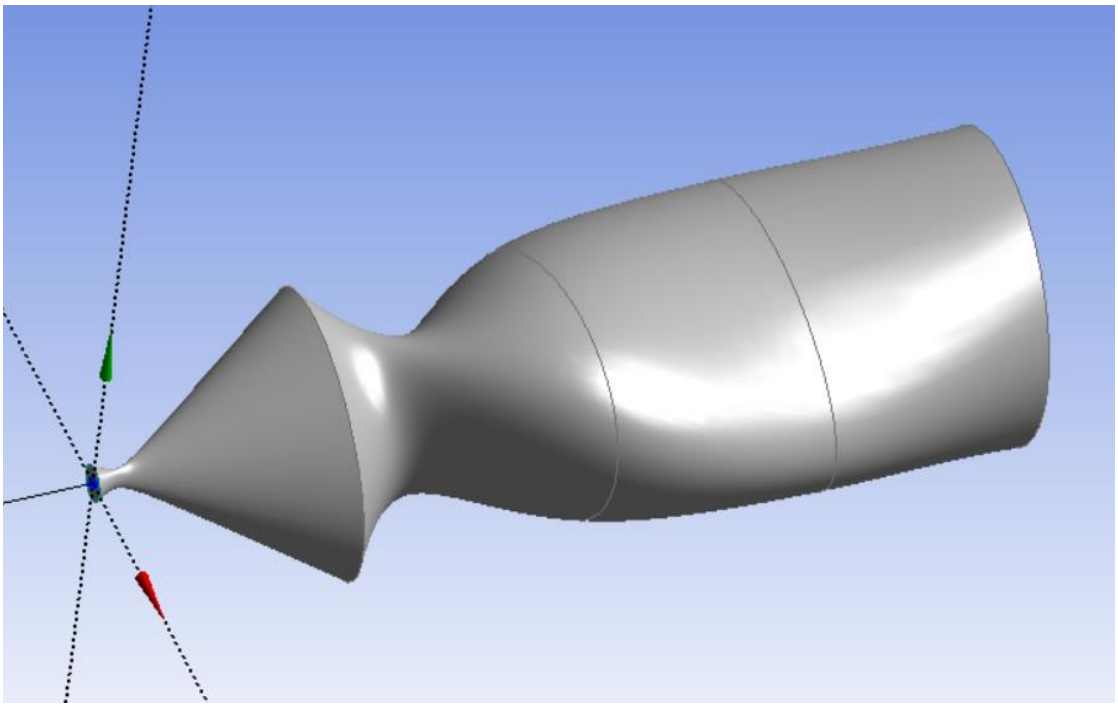

Figure A1.1: Shows the hourglass problem that often occurs when connecting ellipses in Design Modeler

For these reasons, it was deemed impractical to create the heart model from this method.

After some thought, it seemed unlikely that no one had ever done work like this previously. The model shown in Figure A1.2 was found [54].

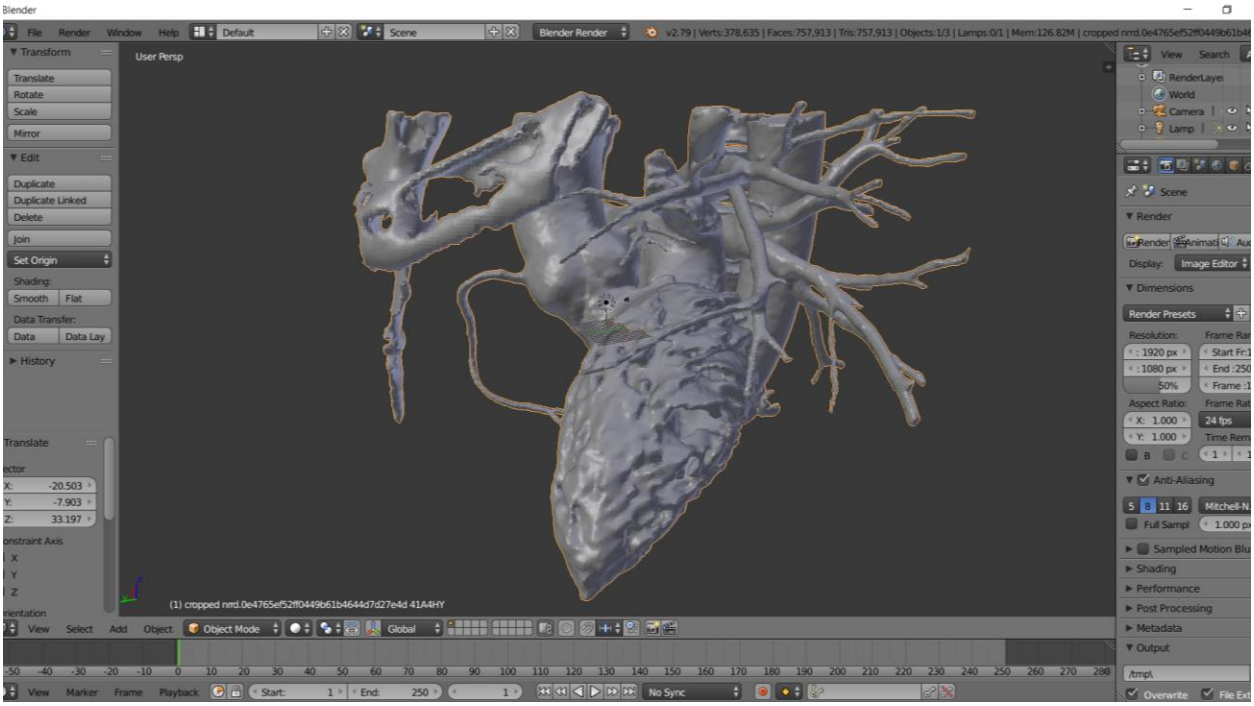

Figure A1.2: A model of the left atrium and ventricle including surrounding blood vessels.

The model is displayed in .stl file editing software Blender [42]. As is, this model contains several structures extraneous to the central question of hemolysis through the artificial heart valve or dehiscence, and so was cleaned up to be more appropriate to the research goals. The results can be found in Figure A1.3.

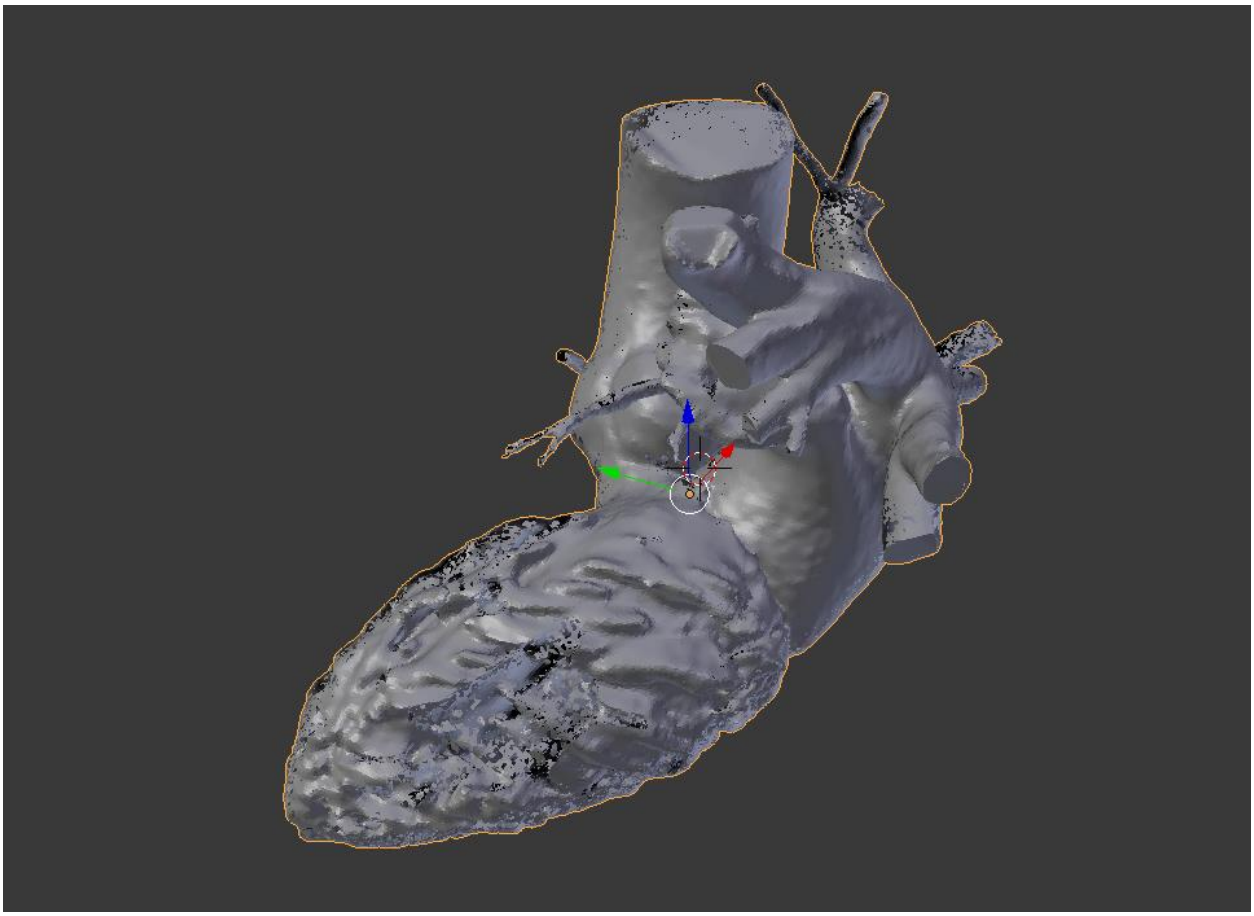

Figure A1.3: A pared down version of the model from Figure A1.2 that removes extraneous structures.

The extra blood vessels and piece of the spine included in the original model have been removed, and now only the pulmonary veins and the aorta remain attached. It was this model that consumed the bulk of the time spent on this project, in an attempt to force it to work properly inside Fluent [36]. There are numerous issues, both with the model itself and originally with the file type it was created as. When the work began, Fluent did not include a way to import .stl files, so the file first had to be converted into a more typical CAD file type. This was undesirable, as .stl files are hollow and therefore relatively small from a file size perspective compared to a solid object of the same magnitude and complexity. This conversion, therefore, resulted in a computationally intensive product that was time-consuming to work with. Mid-project, Fluent was updated with the ability to import .stl files, and this complication disappeared.

The model itself is full of pieces that make it difficult or impossible to properly mesh. Several of the faces overlap, which immediately cancels the meshing process. Furthermore, there are thousands of faces where one or more edges is four orders of magnitude smaller than the others on the same face, or on those of surrounding faces. Effectively meshing these faces is difficult, as making a mesh fine enough to capture these faces requires splitting the larger faces into far too many cells to be practical.

Several solutions were attempted to fix these problems using the tools built into Blender. The limited dissolve tool merges faces that are within a certain angle of each other, combining them into a single face. The tool can be found in Figure A1.4, and the results in Figure A1.5.

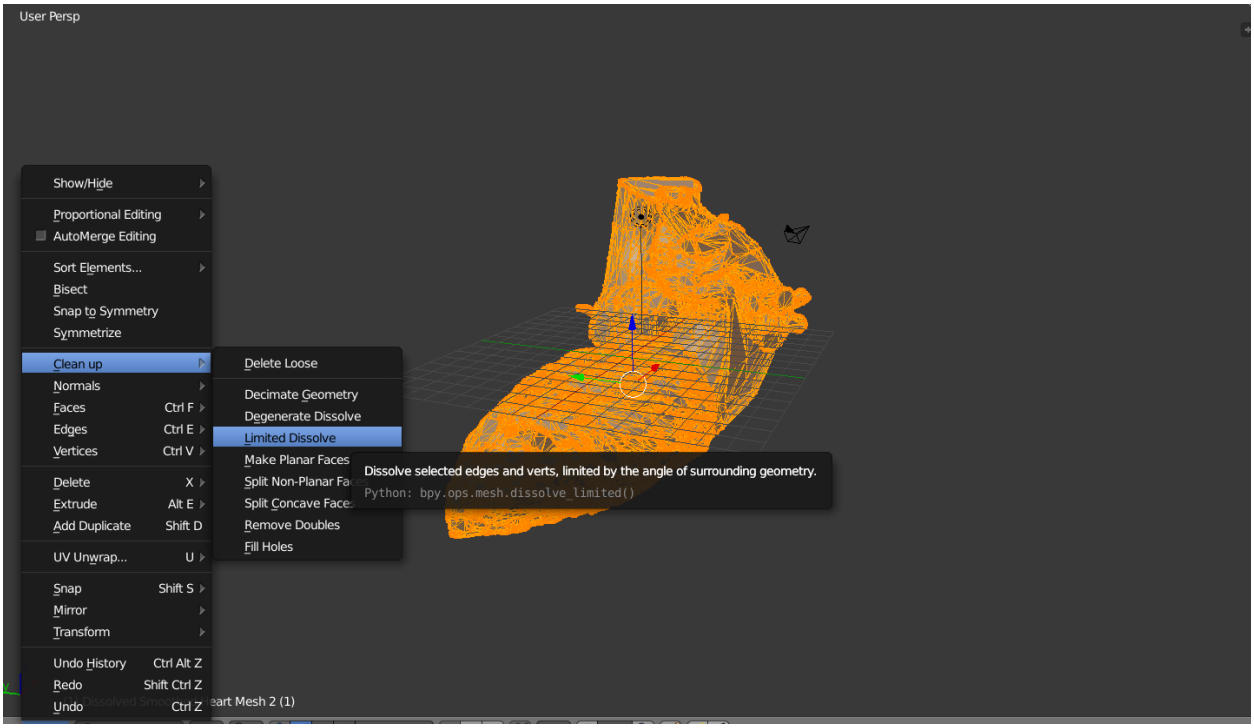

Figure A1.4: The location of the limited dissolve tool

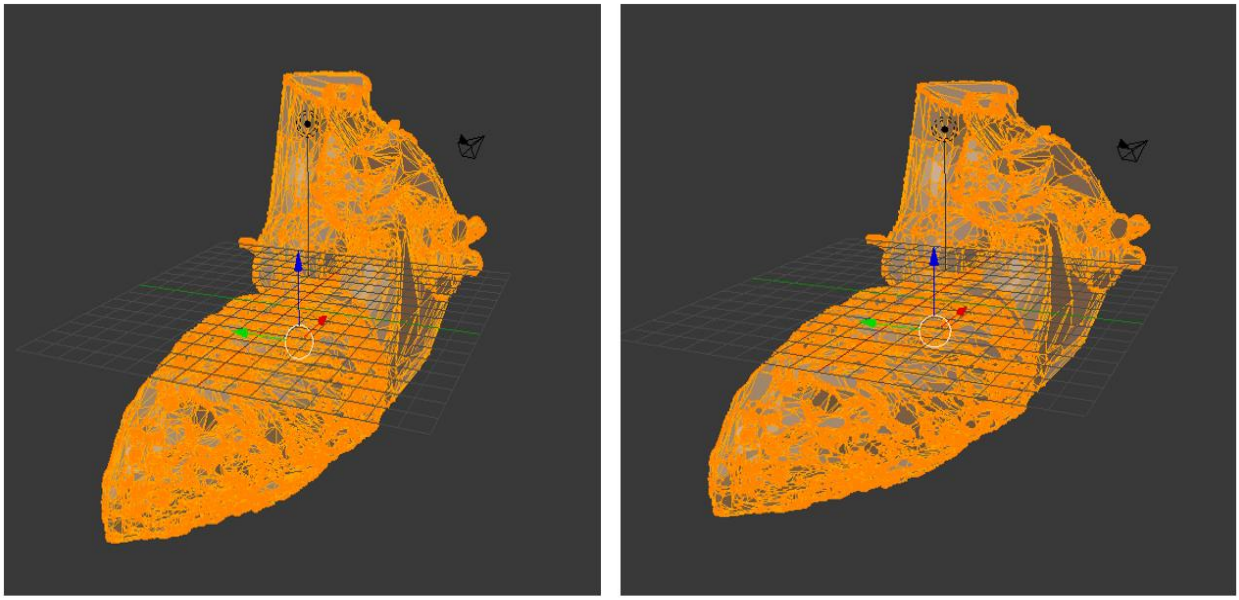

Figure A1.5: A before (left) and after (right) image of the model using the limited dissolve tool. The results are most readily visible on the aorta, where several relatively large faces have been merged, but exist everywhere.

This process has the side effect of creating non-planar faces, but another command located in the same menu as the limited dissolve can fix these, with a net loss to the number of faces. This tool alone was not enough to completely eliminate the problematic faces, and indeed its use made it more difficult to remove them by hand, so a more transformative approach was used. The shrinkwrap feature allows for the creation of a primitive and then matching the vertices of the primitive to the vertices of a model underneath. This removes surface details. This process can

be seen in Figure A1.6.

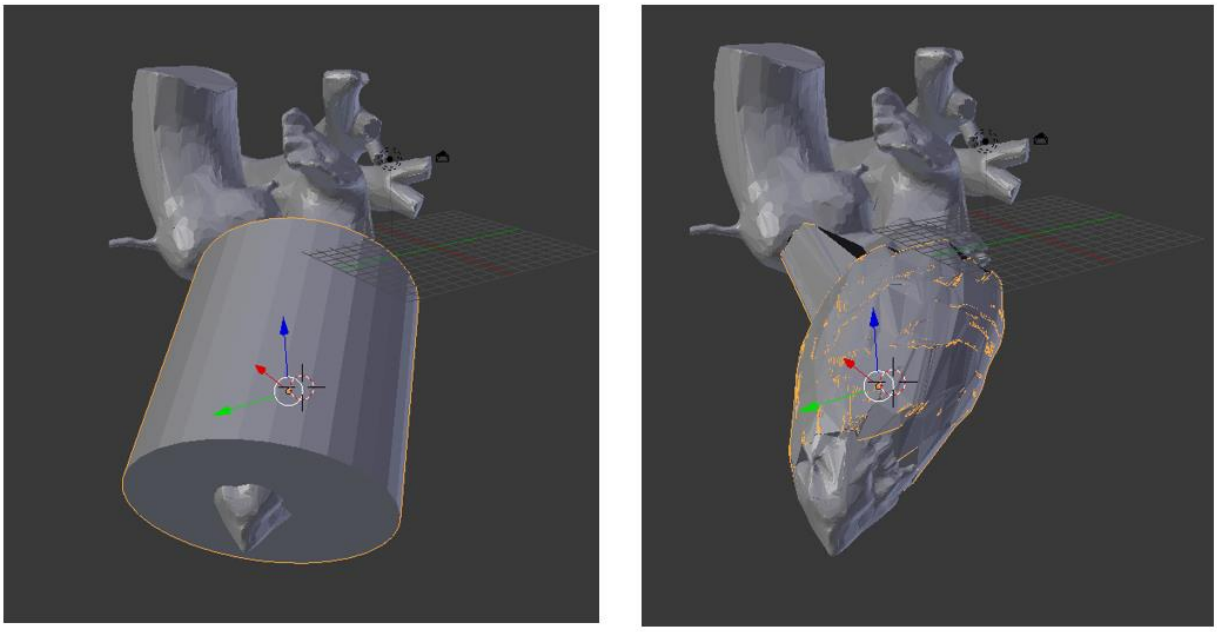

Figure A1.6: A cylinder over the model (left), and that cylinder shrinkwrapped over the ventricle (right).

This is useful for simplifying the surface but introduces two major problems. First, as can be seen in Figure 1A.6 right, the program matches the primitive vertex to the closest model vertex, which can lead to unexpected and erroneous connections, such as the atypical connection between the ventricle and the aorta in Figure 1A.6. The other issue is demonstrated in Figure 1A.7. Very tiny details in the model may be too far from any vertex to have a matching point inside concave depressions. In this case, the shrinkwrap feature will simply cover the detail, instead of erasing it. This creates another set of intersecting faces, which interfere with the ability

to mesh the model.

Figure A1.7: An internal view of the heart model showing a concavity that has not been closed but rather covered by the shrinkwrap feature, leading to overlapping faces and difficulty importing and meshing.

These problems could theoretically all be fixed manually, but the original model has over 700,000 faces. Finding and repairing all the damage was deemed to be too labor intensive after several months of work lead to no significant progress. The next course of action was the creation of the model that was eventually used as described in the Methods section.

Appendix 2

The c code required to implement the Casson viscosity model into fluent via a User Defined Function. The fibrinogen (fibr) and hematocrit (hema) levels vary somewhat for individuals, and could be altered from the present average values [27].

```
#include "udf.h"
DEFINE_PROPERTY(cell_viscosity,c,t)
{
        double fibr = 0.3;

        double hemacrit;

        double hema = 0.4;

        double visc;

        double tauy;

        double muinf;
        double plasamavisc = 0.0167;
        double To = 296.16;
        double T = 310.16;
        double strain;

        double tau;

        if (fibr <= 0.75)
        {
                hemacrit = 0.3126 * pow(fibr, 2) - 0.468 * fibr + .1764;

        }

        else
                hemacrit = 0.0012;
        if (hema > hemacrit)
        {
                tauy = pow(hema - hemacrit, 2) * pow(0.5084 * fibr + .4517, 2);
        }
        else
                tauy = 0;
        muinf = plasamavisc * (1 + 2.073*hema + 3.7222 * pow(hema, 2)) * exp(-7.0276 * (1 - To / T));


        strain = pow(.5,.5) * C_STRAIN_RATE_MAG(c,t);
        tau = pow(pow(tauy,0.5) + pow(muinf * strain, 0.5), 2);
        visc = tau /(10 * strain);
        return visc;
}
```

This function was imported into fluent and tested for a cylindrical system with a periodic boundary condition, for which the expected value of velocity is known. The results of that test

can be seen in Figure A2.1. Note that the C_Strain_Rate_Mag(c,t) command found in the code will return an undefined value if no simulated iterations have been completed, so it is necessary to use a constant viscosity for at least one iteration before this can be implemented. For this research, 100 iterations were completed using a constant value before switching to the user defined function.

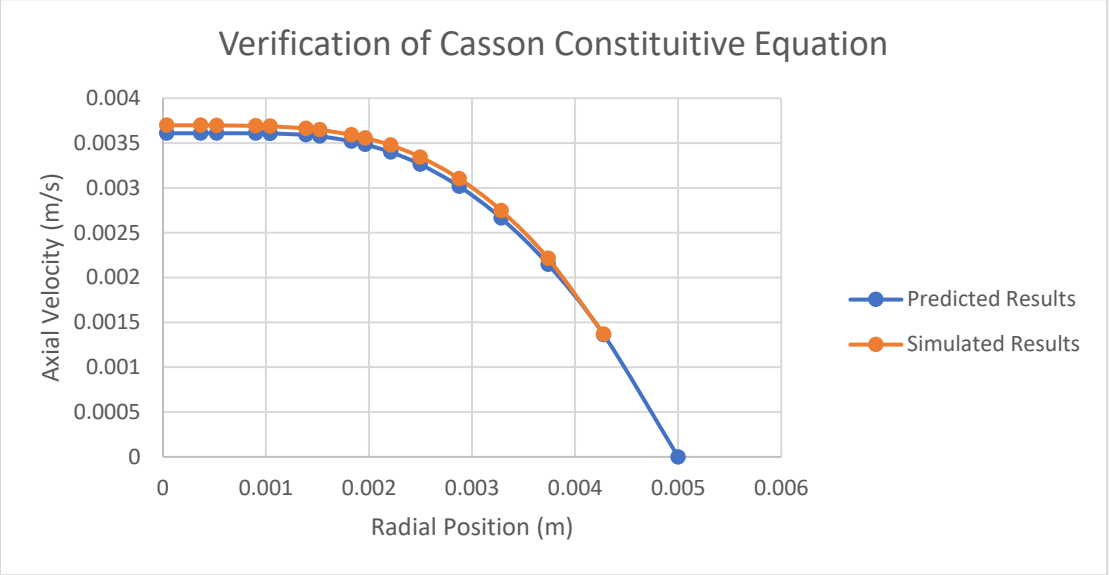

Figure A2.1: Shows the accuracy of the user defined viscosity function in a cylinder.

References

[1] G. Dhaliwal, P. A. Cornett and L. M. Tierney, "Hemolytic Anemia," *American Family Physician,* vol. 69, pp. 2599-2607, 2004.

[2] L. Dean, "Blood Groups and Blood Cell Antigens," Nation Center for Biotechnology Information, 2005. [Online]. Available: https://www.ncbi.nlm.nih.gov/books/NBK2263/table/ch1.T1/. [Accessed 13 November 2020].

[3] A. M. Ali, A. M. Kayani, M. Ali and A. B. Hussain, "Haemolytic Anemia due to Paravalvular Leak Following Mitral and Aortic Valves Replacement," *Journal of ardiovascular Diseases & Diagnosis,* vol. 6, no. 2, 2018.

[4] P. Sethi, G. Murtaza, Z. Rhaman, S. Zaidi, T. Helton and T. Paul, "Valvular Hemolysis Masquerading as Prosethetic Valve Stenosis," *Cureus,* vol. 9, p. e1143, 2017.

[5] R. W. Emery, C. C. Krogh, K. V. Arom, E. A. M., K. Benyo-Albrecht, L. D. Joyce and D. M. Nicoloff, "The St. Jude Medical Cardiac Valve Prosthesis: A 25-Year Experience With Single Valve Replacement," *Cardiovascular,* vol. 79, no. 3, pp. 776-782, 2005.

[6] C. M. Otto and R. O. Bonow, Valvular Heart Disease: A Companion to Braunwald's Heart Disease, Philadelphia, PA: Elsevier Saunders, 2014.

[7] N. Samiei, M. R. Hakimi, Y. Mirmesdagh, M. M. Peighambari, A. Alizadeh-Ghavidel and S. Hosseini, "Surgical outcomes of heart replacement: A study of tertiary specialied cardiac center," *ARYA atheroscelerosis,* vol. 10, no. 5, pp. 233-237, 2014.

[8] National Museum of American History, "Starr-Edwards Heart Valve," Smithsonian Institute, 20 September 2018. [Online]. Available: https://americanhistory.si.edu/collections/search/object/nmah_1726277. [Accessed 19 November 2020].

[9] K. S. Dave, C. K. Madan, B. C. Pakrashi, B. E. Roberts and M. I. Ionescu, "Chronic Hemolysis following Fascia Lata and Starr-Edwards Aortic Valve Replacement," *Circulation,* vol. 46, no. 2, pp. 240-249, 1972.

[10] Y. Shapira, M. Vaturi and A. Sagie, "Hemolysis Associated With Prosthetic Heart Valves A Review," *Cardiology in Review,* vol. 17, no. 3, pp. 121-124, 2009.

[11] L. Haya and S. Tavoularis, "Effects of bileaflet mechanical heart valve orientation on fluid stresses and coronary flow," *J. Fluid Mech.,* vol. 806, pp. 139-164, 2016.

[12] Medical Expo, "Aortic valve prosthesis Regent," Virtualexpo Group, 2020. [Online]. Available: https://www.medicalexpo.com/prod/st-jude-medical/product-70886-527485.html. [Accessed 19 November 2020].

[13] T. Maruyama, Interviewee, [Interview]. 28 February 2020.

[14] Y. Okita, S. Miki and K. Kusuhara, "Propranolol for intractable hemolysis after open heart operation," *Ann Thora Surg,* vol. 52, pp. 1158-1160, 1991.

[15] J. T. Satinga, J. D. Flora and J. B. Rush, "The effect of propranolol on hemolysis in patients with an aortic prosethetic valve," *Am Heart J,* vol. 93, pp. 197-201, 1977.

[16] S. Aoyagi, S. Fukunaga and E. Tayama, "Benefits of a β-blocker for intractable hemolysis due to paraprosthetic leakage," *Asian Cardiovasc Thorac Ann,* vol. 15, pp. 441-443, 2007.

[17] A. Vahanian, H. Baumgartner and J. Bax, "Guidelines on the management of valvular heart disease: the Task Force on the Management of Valvular Heart Disease of the European Society of Cardiology," *Eur Heart J,* vol. 28, pp. 230-268, 2007.

[18] J. M. Jones, H. O'Kane and D. J. Gladstone, "Repeat heart valve surgery: risk factors for operative mortality," *J Thorac Cardiovasc Surg,* vol. 122, pp. 913-918, 2001.

[19] M. Ryomoto, M. Mitsuno, S. Fukui and Y. Miyamoto, "Repair of perivalvular leakage without re-replacement of prosethetic valves," *European Journal of Cardio-thoracic Surgery,* vol. 40, pp. 525-526, 2011.

[20] E. H. Blackstone and J. W. Kirklin, "Death and other time-related events after valve replacement," *Circulation,* vol. 72, pp. 753-767, 1985.

[21] R. J. Cerfolio, T. A. Orszulak, J. R. Pluth, H. W. S. and H. V. Schaff, "Reoperation after valve repair for mitral regurgitation: early and intermediate results," *Journal of Thoracic Cardiovascular Surgery,* vol. 111, no. 6, pp. 1177-1184, 1996.

[22] M. Hourihan, S. B. Perry, V. S. Mandell and e. al., "Transcatheter umbrella closure of valvular and paravalvular leaks," *J Am Coll Cardiol,* vol. 20, pp. 1371-1377, 1992.

[23] M. Genoni, D. Franzen, P. Vogt, B. Seifert, R. Jeni, A. Kunzli, U. Niederhauser and M. Turina, "Paravalvular leakage after mitral valve replacement: improved long-term survival with aggressive surgery?," *Eur J Cardiothorac Surg,* vol. 17, pp. 14-19, 2000.

[24] J. P. Dhasmana, E. H. Blackstone, J. W. Kirklin and N. T. Kouchoukos, "Factors associated with periprosthetic leakage following primary mitral valve replacement," *Ann Thorac Surg,* vol. 35, pp. 170-178, 1983.

[25] I. D. Madukauwa-David, E. L. Pierce, F. Sulejmani, J. Pataky, W. Sun and A. P. Yoganathan, "Suture dehiscence and collagen content in the human mitral and tricuspid annuli," *Biomechanics and Modeling in Machanobiology*, 2018.

[26] G. M. Stiles, K. J. A. and Q. R. Stiles, "Suture technique in preveting dehiscence of prosthetic mitral valves," *Arch Surg*, vol. 121, no. 10, pp. 1136-1140, 1986.

[27] A. J. Apostolidis and A. N. Beris, "Modeling of the blood rheology in steady-state shear flows," *J. Rheology*, vol. 25, pp. 607-633, 2014.

[28] G. B. Thursten, "The elastic yield stress of human blood," *Biomed Sci Instrum*, vol. 29, pp. 87-93, 1993.

[29] S. Chein and K. Jan, "Ultrastructural basis of the mechanism of rouleaux formation," *Microvascular Research*, vol. 5, no. 2, pp. 155-166, 1973.

[30] R. G. Owens, "A new microstructure-based constitutive model for human blood," *J. Non-Newtonian Fluid. Mech.*, vol. 140, pp. 57-70, 2006.

[31] L. B. Leverett, J. D. Hellums, C. P. Alfrey and E. C. Lynch, "Red Blood Cell Damage by Shear Stress," *Biophys. J.*, vol. 12, no. 3, pp. 257-273, 1972.

[32] M. Ozturk, D. V. Papavassiliou and E. A. O'Rear, "An approach of Assessing Turbulent Flow Damage to Blood in Medical Devices," *J. Biomech Eng.*, vol. 139, pp. 011001-011008, 2017.

[33] R. J. Forstrom, "A New Measure of Erythrocyte Membrane Strength- The Jet Fragility Test," *Ph.D. dissertation, University of Minnesota, Minneaspolis, MN*, 1969.

[34] S. P. Sutera and M. H. Mehrjardi, "Deformation and Fragmentation of Human Red Blood Cells in Turbulent Shear Flow," *Biophys. J.*, vol. 15, no. 1, pp. 1-10, 1975.

[35] M. V. Kameneva, G. W. Burgreen, K. Kono, B. Repko, J. F. Antaki and M. Umezu, "Effects of Turbulent Stresses Upon Mechanical Hemolysis: Experimental and Computational Analysis," *ASAIO J.*, vol. 50, no. 5, pp. 418-423, 2004.

[36] "Ansys Fluent," *Release 19.1*.

[37] M. James, "BLOOD DAMAGE ANALYSIS USING COMPUTATIONAL FLUID DYNAMICS OF BLOOD FLOW THROUGH A FUNCTIONING AND MALFUNCTIONING BILEAFLET ARTIFICIAL HEART VALVE," *Thesis*, 2018.

[38] ANSYS, Fluent User's Manual, 2020.

[39] ANSYS, "Design Modeler 19.1".

[40] Z. Xiong, V. V. Fedorov, X. Fu, E. Cheng, R. Macleod and J. & Zhao, "Fully automatic left atrium segmentation from late Gadolinium enhanced magnetic resonance imaging using a dual fully convolutional neural network," *IEE transactions on medical imaging,* vol. 38, no. 2, pp. 515-524, 2019.

[41] P. Andrey and Y. Maurin, "Free-D: an integrated environment for three-dimensional reconstruction from serial sections," *J. of Neuroscience Methods,* vol. 145, pp. 233-244, 2005.

[42] "Blender," *Release 2.79.*

[43] N. M. Katz, B. E. H., K. J. W., B. E. L. and L. J. E., "Suture techniques for atrioventricular valves: experimental study," *J Thorac Cardiovasc Surg,* vol. 81, no. 4, pp. 528-536, 1981.

[44] T. Maruyama, Interviewee, *Suture Diameter.* [Interview]. 23 June 2020.

[45] P. Whelton, R. Carey, A. W.S., D. Casey, K. Collins and C. Himmelfarb, "2017 ACC/AHA/AAPA/ABC/ACPM/AGS/APhA/ASH/ASPC/NMA/PCNA guideline for the prevention, detection, evaluation, and management of high blood pressure in adults: a report of the AMerican College of Cardiology/American Heart Association Task Force of Clinical Pr," *J. Am. Coll. Cardiol.,* vol. 71, no. 19, pp. e127-e248, 2018.

[46] National High Blood Pressure Education Program, The Seventh Report of the Joint National Committee on Prevention, Detection, Evaluation, and Treatment of High Blood Pressure, Bethesda, MD: National Heart, Lung, and Blood Institute, 2003.

[47] E. Braunwald, E. C. Brockenbrough, C. J. Frahm and J. Ross, "Left Atrial and Left Ventricular Pressurein Subjects without Cardiovascular Disease," *Circulation,* vol. XXIV, pp. 267-269, 1981.

[48] F. S. Boretti, J. H. Baek, A. F. Palmer, D. J. Schaer and P. W. Buehler, "modeling hemoglobin and hemoglobin:haptoglobin complexclearance in a non-rodent species-pharmokinetic and therapeutic implications," *Front. Physiol.,* 2014.

[49] Mayo Clinic, "Test Id: PLHBB Plasma Free Hemoglobin, Plasma," Mayo Clinic Laboratories, 2020. [Online]. Available: https://www.mayocliniclabs.com/test-catalog/Clinical+and+Interpretive/9096. [Accessed 12 November 2020].

[50] M. Alkhouli, A. Farooq, R. S. Go, S. Balla and C. Berzingi, "Cardiac Prostheses-related hemolytic anemia," *Clinical Cardiology,* vol. 42, no. 7, pp. 692-700, 2019.

[51] Y. Okita, S. Miki, K. Kusuhara, Y. Ueda, T. Tahata and K. Yamanaka, "Propranolol for Intractable Hemolysis After Open Heart Operation," *Annals of Throacic Surgery,* vol. 52, pp. 1158-1160, 1991.

[52] "Ansys Design Modeller," *Release 19.1*.

[53] National Library of Medicine, "Visible Human Project Gallery," National Institute of Health, 14 August 2015. [Online]. Available: https://www.nlm.nih.gov/research/visible/visible_gallery.html. [Accessed 15 February 2018].

[54] D. Mike, "Left heart atrium and ventricle 1.0.0," Embodi3D, 12 November 2016. [Online]. Available: https://www.embodi3d.com/files/file/7170-left-heart-atrium-and-ventricle/. [Accessed 15 March 2018].

[55] Y. Shapira, M. Vaturi and A. Sagie, "Hemolysis Associated WIth Proesthetic Heart Valves," *Cardiology in Review*, vol. 17, no. 3, pp. 121-124, 2009.

[56] J. P. Dhasmana, E. Blackstone, K. J. W. and N. T. Kouchoukos, "Factors associated with periprosthetic leakage following primary mitral valve replacement: with special consideration of the suture technique," *Ann Thorac Surg*, vol. 35, pp. 170-178, 1983.